

# Origin and significance of early-diagenetic calcite concretions and barite from Silurian black shales in the East European Craton, Poland

MACIEJ J. BOJANOWSKI<sup>1</sup>, ARTUR KĘDZIOR<sup>2</sup>, SZCZEPAN J. PORĘBSKI<sup>3</sup> and MAGDALENA RADZIKOWSKA<sup>1</sup>

<sup>1</sup> ING PAN – Institute of Geological Sciences, Polish Academy of Sciences, Twarda 51/55, PL-00-818 Warszawa, Poland. E-mails: mbojan@twarda.pan.pl; radzikowska@twarda.pan.pl

<sup>2</sup> ING PAN – Institute of Geological Sciences, Polish Academy of Sciences, Research Centre in Cracow, Senacka 1, PL-31-002 Kraków, Poland. E-mail: ndkedzio@cyf-kr.edu.pl

<sup>3</sup> AGH University of Science and Technology, Faculty of Geology, Geophysics and Environmental Protection, Mickiewicza 30, PL-30-059 Kraków, Poland. E-mail: spor@agh.edu.pl

## ABSTRACT:

Bojanowski, M.J., Kędzior, A., Porębski, S.J. and Radzikowska, M.: 2019. Origin and significance of early-diagenetic calcite concretions and barite from Silurian black shales in the East European Craton, Poland. *Acta Geologica Polonica*, **69** (3), 403–430. Warszawa.

The Silurian Pelplin Formation is a part of a thick, mud-prone distal fill of the Caledonian foredeep, which stretches along the western margin of the East European Craton. The Pelplin Formation consists of organic carbon-rich mudstones that have recently been the target of intensive investigations, as they represent a potential source of shale gas. The Pelplin mudstones host numerous calcite concretions containing authigenic pyrite and barite. Mineralogical and petrographic examination (XRD, optical microscopy, cathodoluminescence, SEM-EDS) and stable isotope analyses ( $\delta^{13}\text{C}_{\text{org}}$ ,  $\delta^{13}\text{C}$  and  $\delta^{18}\text{O}$  of carbonates,  $\delta^{34}\text{S}$  and  $\delta^{18}\text{O}$  of barite) were carried out in order to understand the diagenetic conditions that led to precipitation of this carbonate-sulfide-sulfate paragenesis and to see if the concretions can enhance the understanding of sedimentary settings in the Baltic and Lublin basins during the Silurian. Barite formed during early diagenesis before and during the concretionary growth due to a deceleration of sedimentation during increased primary productivity. The main stages of concretionary growth took place in yet uncompacted sediments shortly after their deposition in the sulfate reduction zone. This precompactional cementation led to preferential preservation of original sedimentary structures, faunal assemblages and early-diagenetic barite, which have been mostly lost in the surrounding mudstones during burial. These components allowed for the reconstruction of important paleoenvironmental conditions in the Baltic and Lublin basins, such as depth, proximity to the detrital orogenic source and marine primary productivity. Investigation of the concretions also enabled estimation of the magnitude of mechanical compaction of the mudstones and calculation of original sedimentation rates. Moreover, it showed that biogenic methane was produced at an early-diagenetic stage, whereas thermogenic hydrocarbons migrated through the Pelplin Formation during deep burial.

**Key words:** Carbonate concretions; Stable isotopes; Cathodoluminescence; Sedimentation rate; Marine productivity; Biogenic gas production; Bacterial sulfate reduction; Shale gas.

## INTRODUCTION

The growing realization that organic carbon-rich mudstones may function not only as sources for hy-

drocarbons but also as producible reservoirs has ignited an explosion of interest in such fine-grained rocks. Studies have centered on mudstone composition, fabric, porosity, permeability, organic geochem-

istry, depositional settings and geomechanics (e.g. Ross and Bustin 2009; Passey *et al.* 2010; Slatt 2011; Camp *et al.* 2013; Macquaker *et al.* 2014; Delle Piane *et al.* 2015). Less attention has been paid to carbonate concretions which are commonly hosted by such mudstones.

Carbonate concretions are unique archives of diagenetic processes, as the microtexture, mineralogy, elemental and isotopic compositions of cements in concretions provide a record of the origin and diagenetic evolution of pore waters (Curtis *et al.* 1986; Dix and Mullins 1987; Morad and Eshete 1990; Mozley and Burns 1993; Scotchman 1991; Hudson *et al.* 2001; Hendry *et al.*, 2006). Further crucial information can be obtained from coarse-crystalline cements that formed at different stages of burial, e.g. in septarian cracks (Raiswell *et al.* 2002; Heimhofer *et al.* 2017). Such carbonate concretions, which began to form very close to the sediment-water interface and yet accommodated late-diagenetic cements, may reveal information valuable for evaluation of oil and gas potential, e.g. sedimentation rate (Scotchman 1991; Majewski 2000; Hesse *et al.* 2004; Lash and Blood 2004), microbial methane production (Scotchman 1991; Meister *et al.* 2011; Loyd *et al.* 2012; Bojanowski 2014) or seepage (Ritger *et al.* 1987; Reitner *et al.* 2005) and thermogenic hydrocarbon generation (Hennesy and Knauth 1985; Scotchman *et al.* 2000). Moreover, concretions commonly provide a more realistic picture of the original composition of the sediments and depositional conditions compared to the host rocks, because precompactional cementation effectively protects the components and sedimentary fabrics, which are prone to diagenetic alteration (e.g. McBride 1988; El Albani *et al.* 2001). For instance, even very fragile fossils can be preserved in concretions, whilst they become destroyed in the surrounding sediments (Blome and Albert 1985; Bondioli *et al.* 2015; Cotroneo *et al.* 2016). Furthermore, some part of the original organic compounds can be lost or altered during burial diagenesis of mudstones, whilst they can be preserved in concretions (Kiriakoulakis *et al.* 2000; Pearson *et al.* 2005).

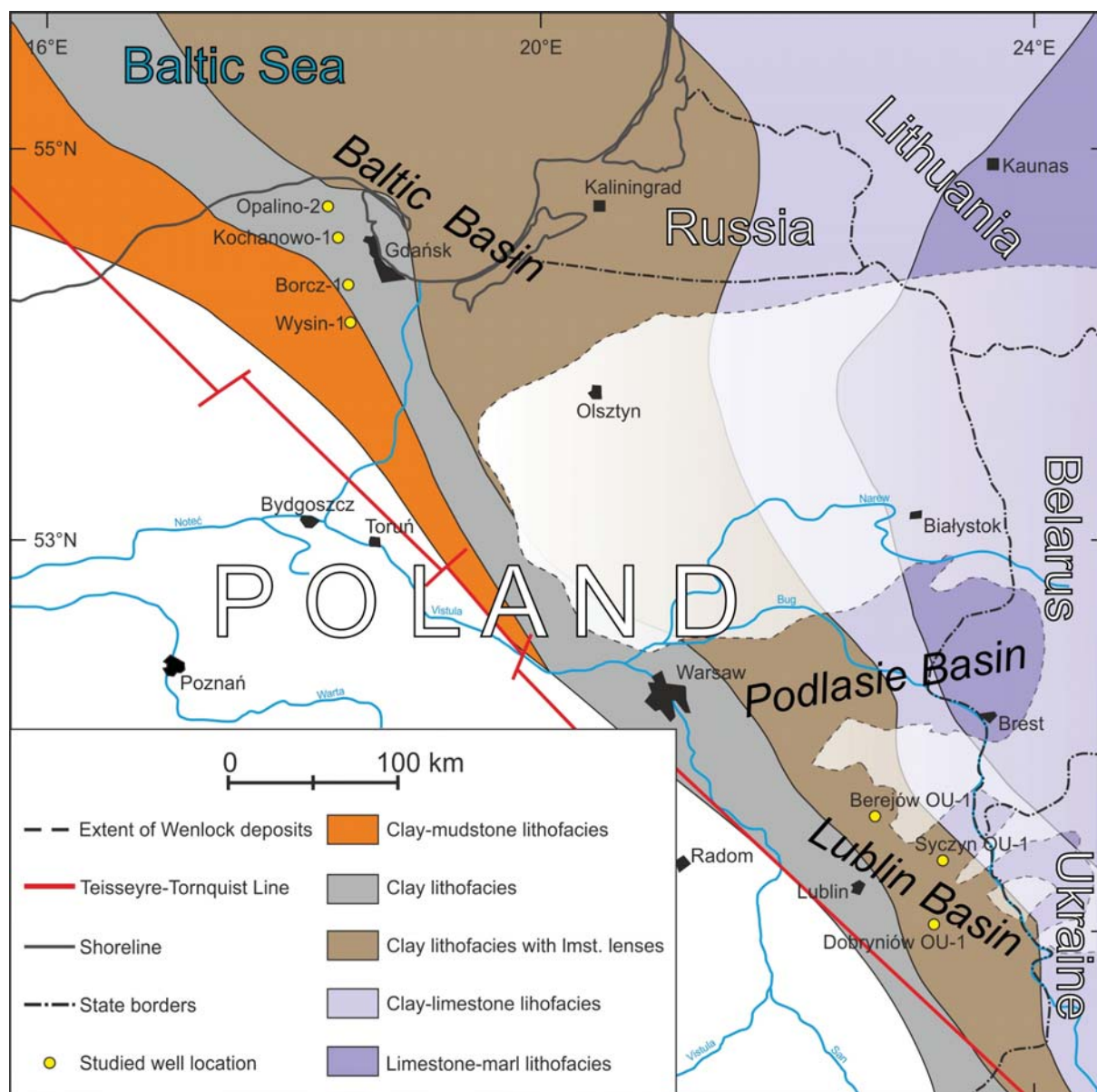
The Silurian dark, organic carbon-rich mudstones from the western margin of the East European Craton in Poland have recently been the target of intensive investigations, as they represent a potential source of shale gas (Poprawa 2010; Więclaw *et al.* 2010). Although the Silurian strata contain numerous carbonate concretions, all studies were focused solely on the host sediments. This contribution is aimed at filling this gap by investigating the mineral, petrographic and geochemical properties of carbon-

ate concretions from Wenlock through Ludlow series in the Baltic and Lublin basins. The main goals of this research are: (1) to recognize the timing and diagenetic setting of concretionary growth, (2) to characterize the sources of parent fluids and bicarbonate for concretionary cements, (3) to unravel the diagenetic processes that affected the mudstones, and finally (4) to identify the paleoenvironmental conditions, which induced such extensive authigenesis over a prolonged time period (~10 Myrs) in basins that were ~500 km apart. The results of our work demonstrate the high value of carbonate concretions for the understanding of salient characteristics of shale gas play.

## GEOLOGICAL SETTING

The studied concretions occur in the Pelplin Formation forming part of a Silurian mud-prone wedge, which stretches along the western margin of the East European Craton (EEC) between southern Scandinavia, Poland and Ukraine (Text-fig. 1). The wedge is interpreted as the distal fill of a Caledonian foredeep that originated due to the collision of East Avalonia with Baltica (Poprawa *et al.* 1999; Jaworowski 2000; Giese and Köppen 2001; Poprawa 2006). The fill thins and onlaps eastwards the EEC. Westwards, it contacts with the Caledonian thrust front in the Baltic sector (Mazur *et al.* 2016), whereas farther to the south, the basin-fill is concealed under the Mesozoic–Cenozoic sediment pile in central Poland. The foredeep fill is broken-up by later tectonic and erosional activity into three areas referred to as the Baltic, Podlasie and Lublin basins (Poprawa 2010), each showing a broad mudrock belt that passes laterally cratonwards into a carbonate shelf ramp (Modliński 2010).

The Silurian succession is up to 3800 m thick and subdivided into a number of lithostratigraphic units (Text-fig. 2; Modliński *et al.* 2006). It starts with the Pasłek Formation (Llandovery), which onlaps Ordovician carbonates to the east across a transgressive ravinement unconformity (Porębski *et al.* 2013). The basal Jantar Member (Rhuddanian–early Aeronian) of the Pasłek Formation consists mainly of black, graptolitic, organic carbon-rich, argillaceous to locally siliceous mudstones. They become interbedded on a cm-scale with green, organic carbon-lean bioturbated mudstones, bentonites, and rare carbonate concretions upwards throughout the formation (Telychian). The Jantar Mudstone records the deglacial (post-Hirnantian) anoxia (Podhalańska

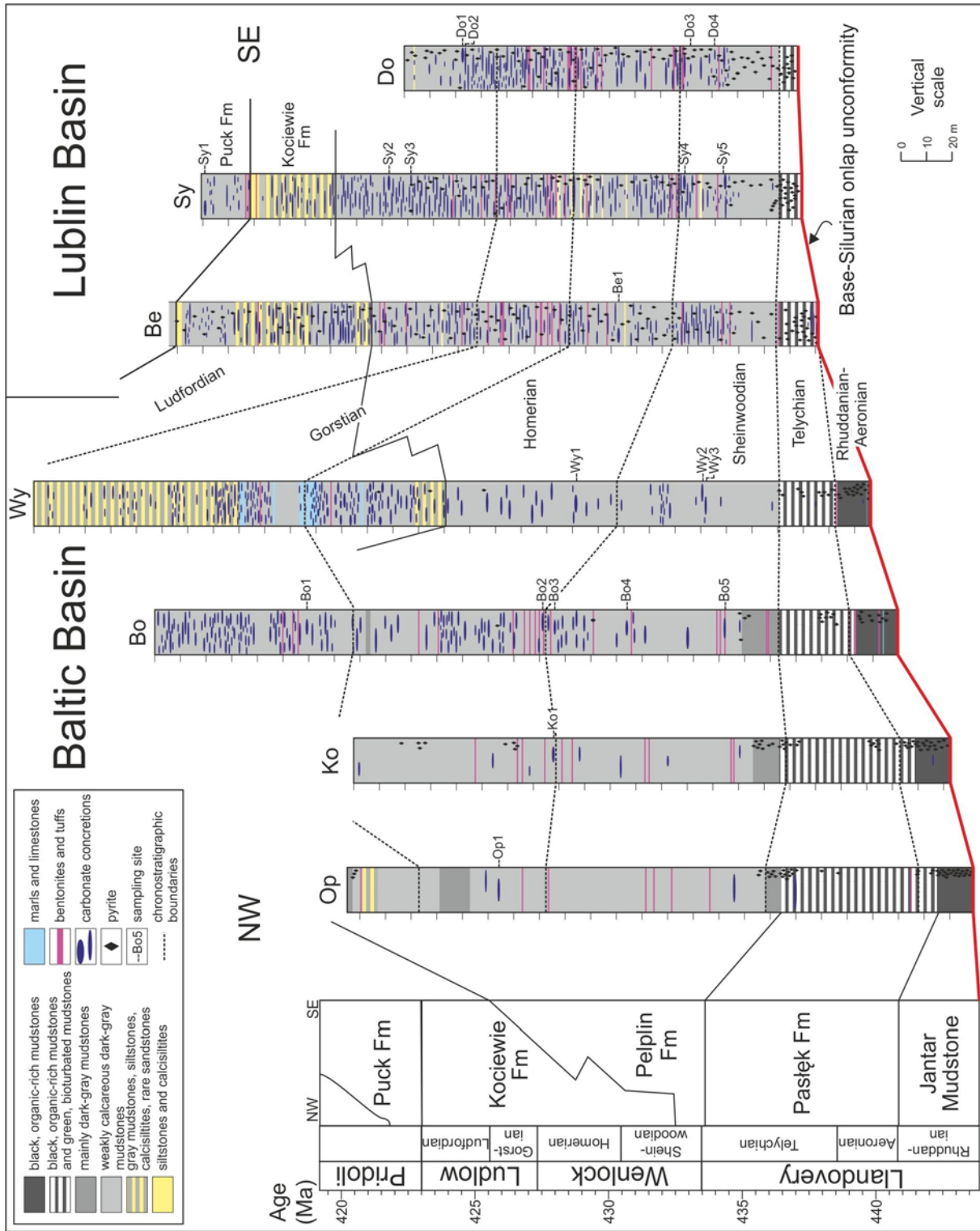


Text-fig. 1. Wenlock lithofacies map (modified from Modliński, 2010) with the locations of studied wells

2009), as seen similarly at many locations around the Rheic Ocean (e.g. Lüning *et al.* 2000). The alternation of bioturbated and unbioturbated intervals in the Telychian reflects intermittent anoxic-oxic near-bottom conditions due most likely to glacioeustatically-driven changes in oceanic circulation patterns generated during the Early Paleozoic Icehouse (cf. Page *et al.* 2007; Trela *et al.* 2016). The Pasłęk Formation occurs as a basinwide sheet, up to 80 m thick, which was deposited at upper bathyal to outer

neritic depths (Modliński and Podhalańska 2010) during the underfilled foredeep stage.

These mudstones pass upwards rather abruptly into the Pelplin Formation (Sheinwoodian–Ludfordian) that is particularly rich in carbonate concretions. This formation is dominated by grey to black, laminated argillaceous, often pyritiferous mudstones with calcite and dolomite and intercalated with thin bentonites. Siliciclastic and calcareous silt lenses, solitary laminae and occasional laminasets as well as



Text-fig. 2. Generalized stratigraphy of the Silurian mudrock belt in the western part of the East European Craton (modified from Modliński *et al.* 2006 and Podhalańska *et al.* 2010) and lithological logs of cored well intervals, showing the locations of studied samples. Silurian chronostratigraphy is after Melchin *et al.* (2012)

mm-thick lags of finely comminuted shelly matter, comprised mostly of echinoid stems, appear as subordinate components. These grow in frequency upwards in the Pelplin Formation. Faunal assemblages are dominated by graptolites often accompanied by nautiloids, but levels enriched in benthic fauna, mostly small-sized brachiopods, bivalves and ostracods, reappear episodically in the formation particularly in the Lublin Basin. The lithological variability and bedding style point to the frequent interruption of slow settling of mud by episodes of deposition from fast-moving muddy suspensions, most likely storm-generated flows (Dziadzio *et al.* 2017).

The Pelplin Formation grades upwards and laterally (to the NW) into grey, graptolitic, dolomitic and calcareous, massive and laminated mudstones, which are interbedded with frequent siltstones, carbonate concretions, bentonites and rare sandstones. These sediments constitute the Kociewie Formation (mid-Sheinwoodian–Ludfordian), which is a synorogenic wedge supplied from the Caledonian accretionary prism to the NW and W (Jaworowski 2000; Poprawa 2006). Both mudstones and coarser-grained sediments provide evidence of event deposition from turbidity currents, storm-generated currents and traction currents (Jaworowski 1971, 2000; McCaan 1996; Modliński and Podhalańska 2010). The presence of micro-hummocky cross-stratification, gutter casts and combined-flow mud ripples (Porębski *et al.* 2013) suggests shallowing into middle neritic depths (offshore-shelf transition zone). The Pelplin and Kociewie formations attain 3500 m in thickness and record the filled stage in foredeep evolution during Wenlock–Ludlow times. These formations are overlain by the Pridoli Puck Formation, which has poor core coverage and appears dominated by calcareous mudstones.

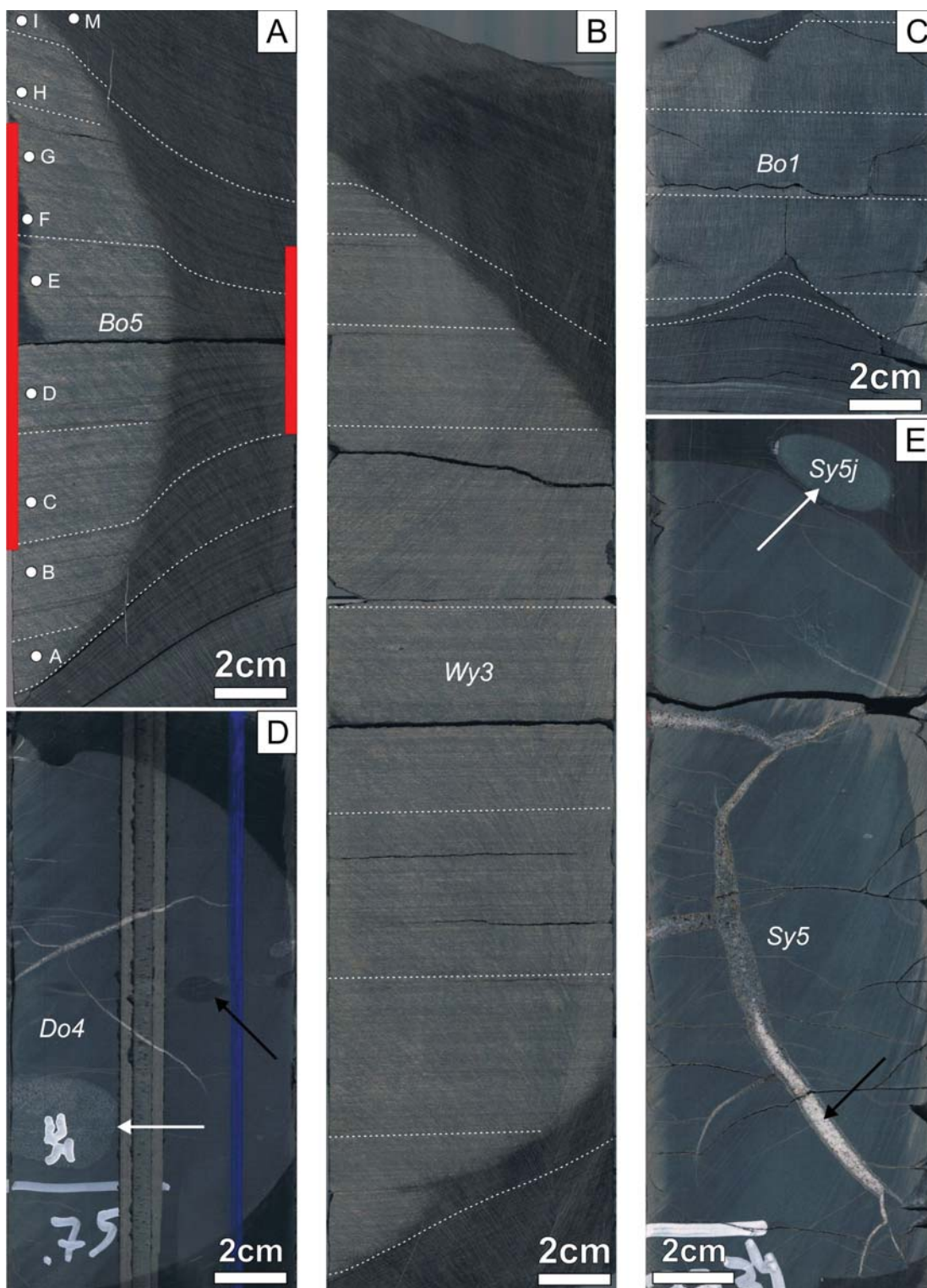
## MATERIAL AND METHODS

Twenty specimens of concretions were collected together with the surrounding mudstones. Nineteen specimens were collected from the Wenlock–Ludlow series of the Pelplin Formation, whilst one (Sy1) came from the Pridoli Puck Formation (Text-fig. 2). The material was collected from drill cores from seven wells in the depth range between 2 and 4 km. Each specimen is given a symbol composed of the first two letters of the well name and a consecutive number. Wells Syczyn OU-1, Dobryniów OU-1 and Berejów OU-1 were drilled in the Lublin Basin, and Borczy-1, Wysin-1, Opalino-2 and Kochanowo-1 in the western

Baltic Basin (Text-fig. 1). The dip of the Silurian strata in the cores studied was negligible. The cores were cut along vertical planes which allowed macroscopic examination and precise collection of samples with a microdrill (Text-fig. 3A). From one to three uncovered polished thin sections per concretion were cut from the vertical sections, forty two in total. At least one was cut from the edge of each concretion together with the surrounding mudstone.

The thin sections were studied using a Nikon Eclipse LV100POL polarizing microscope and a CITL Mk5-2 cold cathode device operating at ~17 kV beam energy, ~0.3 mA beam current and 0.003 mBar vacuum combined with a polarizing microscope Nikon Eclipse 80i at the Institute of Geological Sciences, Polish Academy of Sciences (ING PAN) in Warsaw, Poland. Then, high-resolution observations and analyses of mineral and elemental compositions were made by scanning electron microscopy (SEM) analysis using a ZEISS Sigma VP FE-SEM (variable pressure field emission scanning electron microscope) at the Faculty of Geology, University of Warsaw. Ten thin sections were polished and un-coated and were analyzed at 50 Pa for charge compensation by nitrogen gas in the SEM chamber. Electron beam acceleration voltage of 20kV was set for imaging and EDS analyses. The SEM probe current is estimated to greatly exceed 10nA. BSE images were taken with an angularly selective BSE (AsB™) detector permanently attached to the end of the e-beam column. EDS analyses were collected with two Bruker XFlash 6|10 SDD type detectors.

Powdered samples were collected using a hand-held *Dremel 3000* rotary tool equipped with sintered diamond microdrills along transects from the base to the top of a concretion and numbered with a suffix alphabetically beginning with “a” at the base (Text-fig. 3A). Bo1 specimen was sampled along a horizontal transect as well, because it is composed of two coalesced concretions (Text-fig. 3C). An additional sample (Sy5j) was collected from a small barite-calcite concretion lying above the main concretion in the Sy5 specimen (Text-fig. 3E). One mudstone sample was taken from each specimen except Bo4 which did not contain the surrounding material. The mudstone samples are marked with a “m” suffix. Coarse-crystalline septarian cements were also sampled from six concretions and marked with a „s” suffix followed by numbers according to their order of precipitation. The mineral composition of 50 samples (19 mudstone and 31 concretion samples) was determined with XRD using a Bruker D8 ADVANCE



Text-fig. 3. Cross-sections of cores illustrating the internal structure of the concretions. A-C – Concretions with lamination from the Baltic Basin. Note differential compaction and lamination styles (dashed lines) in mudstones and concretions. Red bars in A show the thickness of the same lamina sets occurring in a concretion and mudstones. Lamination within concretions is plane parallel, except A, where slight inclination is observed in the top and bottom parts. Some concretions may be coalesced (C). White circles in A indicate location and diameter of spots where subsamples were drilled. D-E – Homogeneous concretions with septarian cracks and domains with small barite crystals (white arrows) from the Lublin Basin. Black arrows indicate a bivalve in D and a coarse barite filling central parts of a septarian crack in E

diffractometer in a Bragg-Brentano system at ING PAN. Modeling of the contents of crystalline phases was performed by the Rietveld method.

Stable C and O isotope ratio measurements were performed by reacting carbonate powders with 104% orthophosphoric acid at 70°C using a Thermo KIEL IV Carbonate Device connected on-line to a Thermo-Finnigan Delta Plus mass spectrometer in a Dual Inlet system. Measurements of the NBS19 standard were conducted after 10 successive measurements of samples. The accuracy of the measurements ( $1\sigma$ ) was  $\pm 0.03\text{‰}$  for  $\delta^{13}\text{C}$  and  $\pm 0.07\text{‰}$  for  $\delta^{18}\text{O}$ . All values are reported as  $\delta^{13}\text{C}_{\text{carb}}$  and  $\delta^{18}\text{O}_{\text{carb}}$  in per mil relative to V-PDB by assigning a  $\delta^{13}\text{C}$  and  $\delta^{18}\text{O}$  values +1.95‰ and -2.20‰ to NBS19. The  $\delta^{18}\text{O}$  values of mudstones, which are rich in dolomite (with dolomite/calcite ratio  $>0.1$ ), were corrected using the phosphoric acid fractionation factor given by Rosenbaum and Sheppard (1986). Correction was applied proportionally to dolomite/calcite ratio obtained with X-ray diffractometry (XRD). Since the dolomite/calcite ratio in the concretions does not reach 0.1, such correction was not applied for these samples.

$\delta^{13}\text{C}_{\text{org}}$ ,  $\delta^{34}\text{S}_{\text{sulf}}$  and  $\delta^{18}\text{O}_{\text{sulf}}$  were determined using a Thermo Flash EA 1112HT elemental analyzer connected to a Thermo Delta V Advantage isotope ratio mass spectrometer in a Continuous Flow system. Carbonates were leached from the samples prior to isotopic measurements by reacting them with 5% HCl at room temperature. The resultant solution was rinsed with distilled water several times until the initial pH of water was reached. After centrifugation and decantation, the residue was split into two portions, which were dried at 40°C for 2 to 3 days (for  $\delta^{13}\text{C}_{\text{org}}$  measurements) and at 105°C for 24 hours (for  $\delta^{34}\text{S}_{\text{sulf}}$  and  $\delta^{18}\text{O}_{\text{sulf}}$  measurements). For C and S isotope measurements, the samples were wrapped in tin capsules and combusted in the elemental analyzer at 1020°C, whereas for O isotope measurements, the samples were wrapped in silver capsules and pyrolyzed at 1450°C. Released gases were transferred to the spectrometer source through a capillary. C, S and O isotope compositions are reported as  $\delta^{13}\text{C}_{\text{org}}$ ,  $\delta^{34}\text{S}_{\text{sulf}}$  and  $\delta^{18}\text{O}_{\text{sulf}}$  values relative to VPDB, VCDT and VSMOW, respectively and normalized to calibration curves based on analyses of international standards (three standards for each isotope ratio). Precision of the measurements was monitored by replicate analysis of laboratory standards and is better than  $\pm 0.12\text{‰}$ ,  $\pm 0.3\text{‰}$  and  $\pm 0.5\text{‰}$  ( $1\sigma$ ) for  $\delta^{13}\text{C}_{\text{org}}$ ,  $\delta^{34}\text{S}_{\text{sulf}}$  and  $\delta^{18}\text{O}_{\text{sulf}}$ , respectively. All stable isotope measurements were performed at the Stable Isotope Laboratory at ING PAN in Warsaw.

## RESULTS

### Macroscopic observations

Calcite concretions are conspicuous features in the mudstones examined, where they occur in large numbers. A 207-m long core interval encompassing the concretion-bearing interval in the Syczyn OU-1 well contains 256 concretions which make up ~21 meters of core in total. Thus, concretions constitute on average ~10% of the core in the entire concretion-bearing interval, but they are particularly abundant in a 100 meters thick interval that belongs to the Pelplin Formation, where they comprise ~15%. Frequency of concretion occurrence in a time frame is similar in Borcz-1, Berejów OU-1, Syczyn OU-1 and Dobryniów OU-1 wells (60–70 specimens in the Wenlock), Wysin-1 exhibits almost twice as much, whereas concretions are rare in Opalino-2 and Kochanowo-1 (Text-fig. 2). However, the number of concretions per meter of core is evidently higher in the Lublin than in the Baltic Basin due to reduced thicknesses of the Silurian deposits in the former. The Wenlock deposits in the Lublin Basin are ~80 m thick, whereas they are more than twice as thick in the Baltic Basin, which gives mean accumulation rates of 13 mm/kyrs for the Lublin and 23–31 mm/kyrs for the Baltic basins.

The concretions exhibit quite regular shapes with aspect ratios from subspherical to ellipsoidal (Text-fig. 3). However, some specimens display rather irregular and unusual morphologies, some of which may result from coalescence of two or more concretions (Text-fig. 3C). All concretions from the Baltic and many from the Lublin Basin exhibit lamination (Text-fig. 3A–C). The concretions with lamination are always associated with thinly laminated mudstones, whilst the homogenous concretions from the Lublin Basin are associated with massive or indistinctly laminated mudstones. The laminae of the mudstones are bent around the concretions and strongly inclined ( $<45^\circ$ ) due to differential compaction, whereas the lamination is plane parallel, roughly horizontal and not deformed even at the edges of most concretions (Text-fig. 3B, C). Three concretions (Bo3, Bo5 and Ko1) exhibit lamination that is inclined in their outer parts (Text-fig. 3A). Individual laminae can be traced beyond the concretions, where they become markedly thinner. The thickness of a given concretion is 2 to 3 times larger than that of the corresponding laminae set in the mudstones (Text-fig. 3A). Therefore, the mean accumulation rates calculated above, should be multiplied by 3, which gives the original sedimenta-

tion rates for uncompacted sediments of ~4 cm/kyrs for the Lublin Basin and ~9 cm/kyrs (Wysin-1 and Borcz-1 wells) for the Baltic Basin. These estimates should be treated as minimum values, as the thickest parts of large concretions were not represented in the cores that are <8 cm in diameter.

The body of the concretions is composed of a fine carbonate matrix that is grey, but paler than the mudstones. Certain laminae are composed of more coarse-grained detrital material or densely packed with macrofossils cemented with sparite representing storm deposits. Some parts of several concretions contain abundant scattered pyrite. Prismatic, up to 10 mm long barite crystals are found in some concretions. These crystals either occur along some horizons as shrub-like clusters, form oval domains in the center of concretions (Text-fig. 3D) or occur as separate small barite-calcite concretions (Text-fig. 3E). Barite was not found in the surrounding mudstones. Septarian fractures cut through the concretion body, pyritized areas and barite domains in some specimens. The fractures are widest in the center and taper out towards the edges of the concretions, rarely reaching the outer surface (Text-fig. 3D, E).

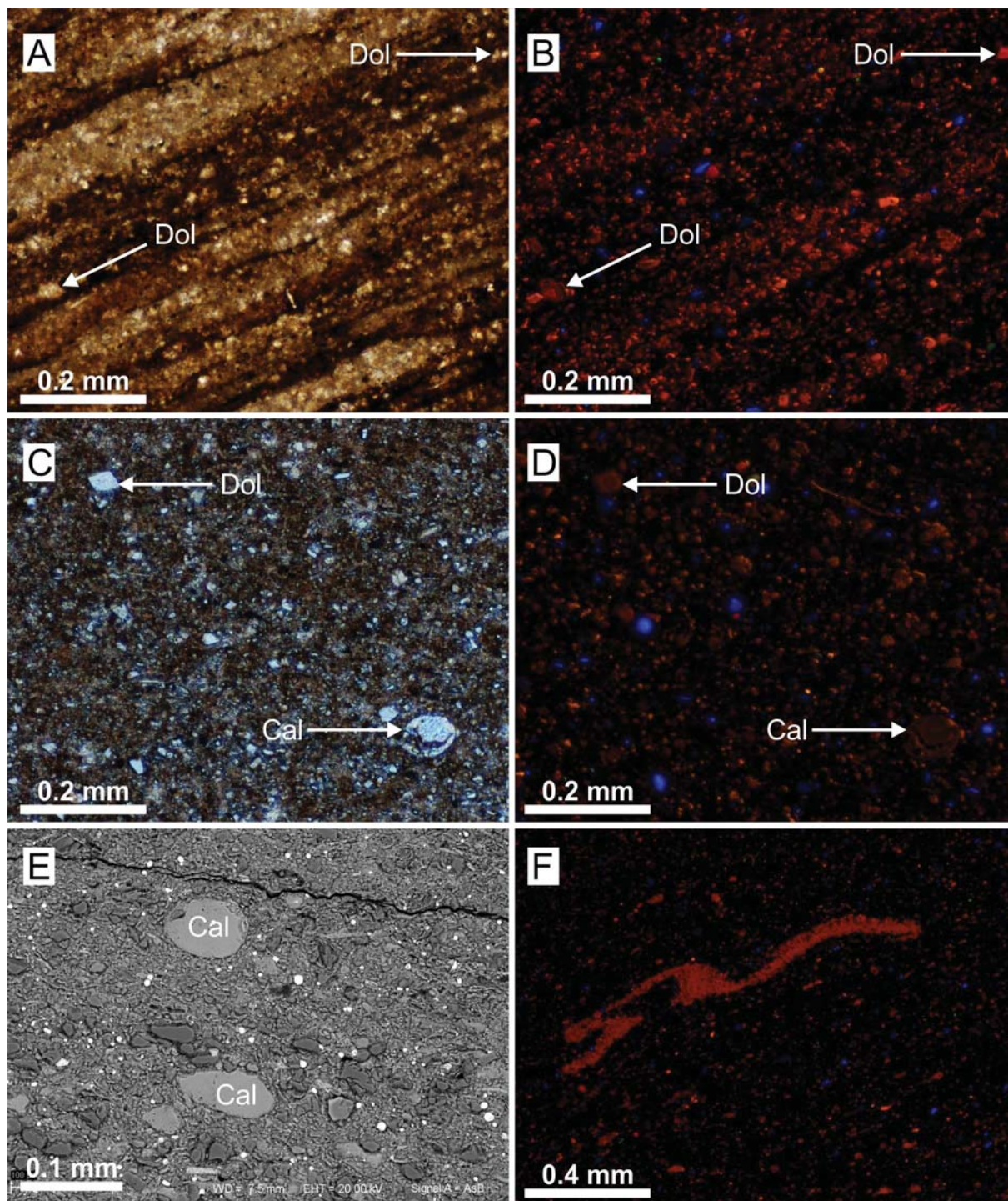
### Mineral composition

The main mineral components of the mudstones are quartz (23–39%), 2:1 layer phyllosilicates comprising muscovite, illite and/or mixed-layer illite-smectite (13–32%), chlorite (12–21%), albite (8–15%), pyrite (2–8%) and carbonates (<24%) comprising calcite <10% and/or dolomite <17% (Suppl. Table 1; all supplementary tables are available only in online version). Dolomite/calcite ratio varies up to 3. Quartz/2:1 layer phyllosilicates ratio varies from 0.8 to 3.0 and is higher in the Baltic (1.8 on average) than in the Lublin Basin (1.2 on average). Sample Do3m has exceptionally high carbonate (45%) and low quartz contents (11%). Sample Do1m is exceptionally rich in pyrite (14%). K feldspars (<8%), kaolinite (3 and 8% in two samples) and gypsum (2% in one sample) occur only occasionally. Gypsum is probably a product of pyrite oxidation. Bodies of the concretions are composed of the same set of minerals, but in far different proportions. Calcite is the dominant component of the concretions, as it comprises 68–91%. Comparison of calcite content between the concretions and the surrounding mudstones indicates four- to seven-fold dilution of the primary detrital material by the concretionary cement. Barite was detected by XRD in one concretion (7% in sample Do4d).

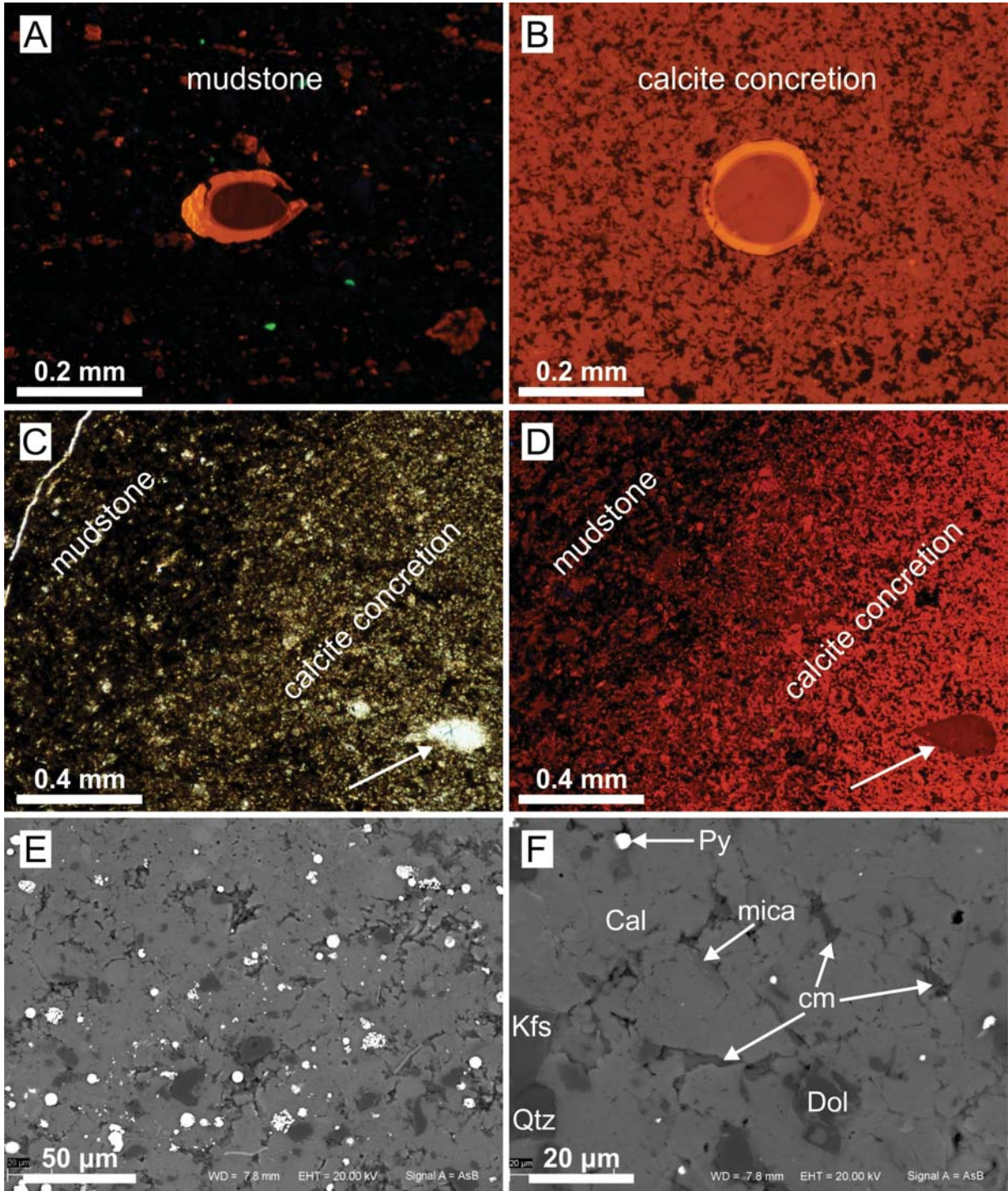
### Petrography and elemental composition

Results of microscopic examination and EDS analyses are given in Suppl. Tables 2 and 3, respectively. The mudstones are commonly thinly laminated and rich in organic matter and framboidal pyrite with diameters mostly <10 µm, but up to 30 µm. The lamination results from variation in organic matter and detrital material contents (Text-fig. 4A and B). Some laminae exhibit micronodular fabric due to the abundance of lenticular, carbonate-rich pellets. The siliciclastic material is clay- to silt-sized. Carbonate particles are mostly silt-sized, high-Mg (<8.2 mol%), anhedral calcite grains with Mn contents below EDS detection (probably intraclasts) with a weak orange or dull luminescence (Text-figs 4 and 5). Carbonate bioclasts were identified only in several samples and they are mostly corroded microfossils in the shape of flattened spheres ~0.1 mm in diameter (Text-figs 4C–E and 5A). A supposed macrofossil (corroded trilobite) was found in only one sample (Text-fig. 4F). Calcite cement is rare and it mostly fills microfossils (Text-figs 4C–E and 5A). Intergranular microspar cement having uniform elemental composition (~5.0 mol% of Mg, ~0.2 mol% of Mn and ~2.4 mol% of Fe) and dull luminescence (Text-fig. 5A) was identified in a few samples, but considerable quantities were observed only in Do3m. Dolomite, which is a more common authigenic phase in the mudstones, is Fe-rich (~2.5 mol%) and developed as zoned rhombohedra <60 µm across (Text-fig. 4).

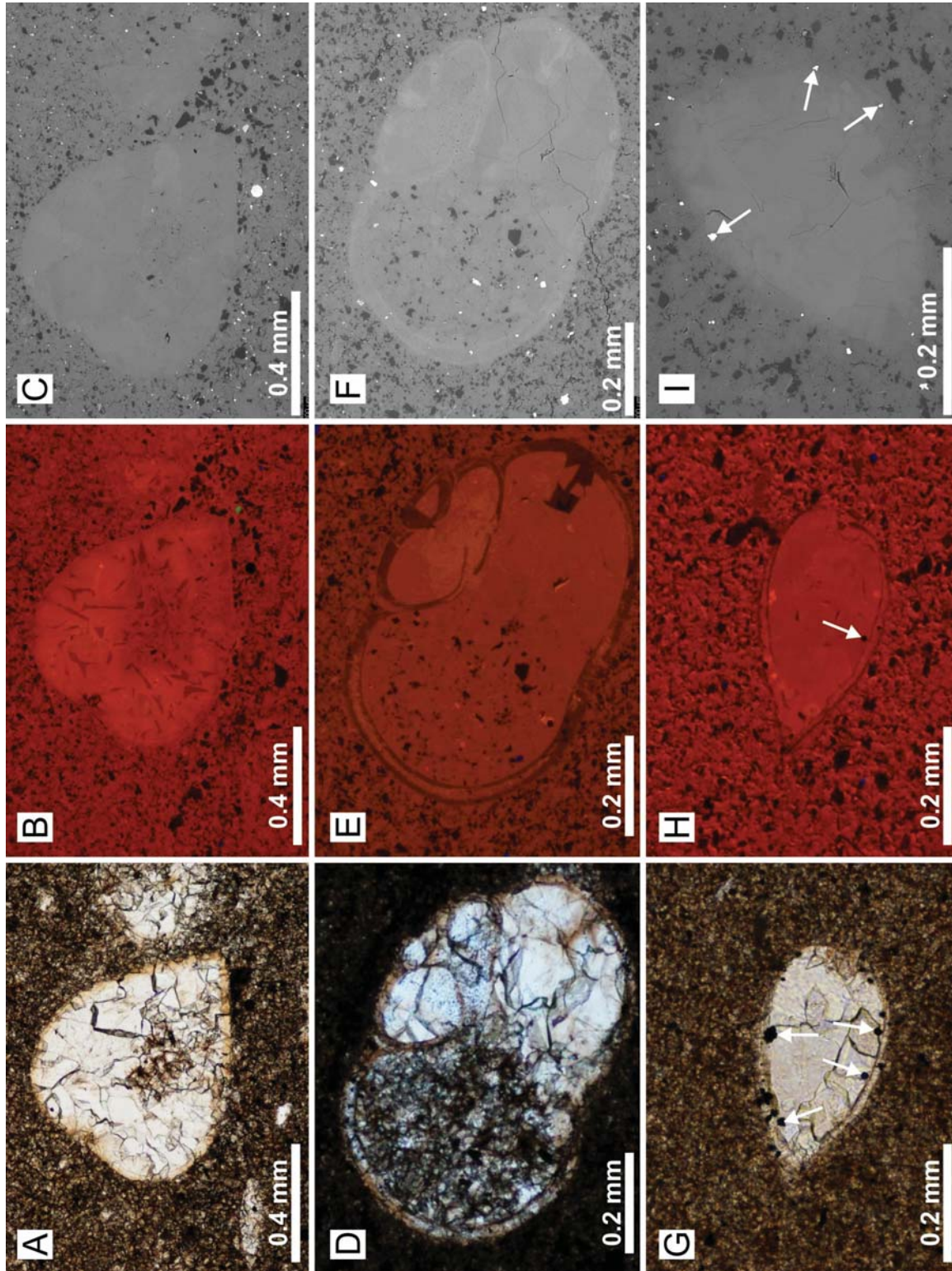
All components observed in the mudstones, occur also in the concretions, except that the microfossils are not flattened (Text-fig. 5B). Detrital material is tightly cemented by anhedral concretionary calcite microspar (5–40 µm) with a variable elemental composition, but uniform micromorphology within each concretion (Text-fig. 5E and F). Micromorphology does not vary between the concretions as well. The only exception was observed in the basal part of concretion Do3, where concretionary calcite is much coarser-crystalline (<400 µm) and accompanied by large cubic pyrite; both features probably related to recrystallization. Concretionary microspar contains 1.2–5.9 mol% of Mg (3.9 on average), <0.6 mol% of Mn (0.2 on average) and <1.9 mol% of Fe (0.9 on average) and exhibits strong luminescence (orange to red) that is brighter than that of carbonate grains in the mudstones, probably due to the very low Mn content in the latter (Text-fig. 5C and D). Detrital material in the concretions is dispersed and intergranular contacts are rarely observed (Text-fig. 5E and F), which may suggest displacive cement growth.



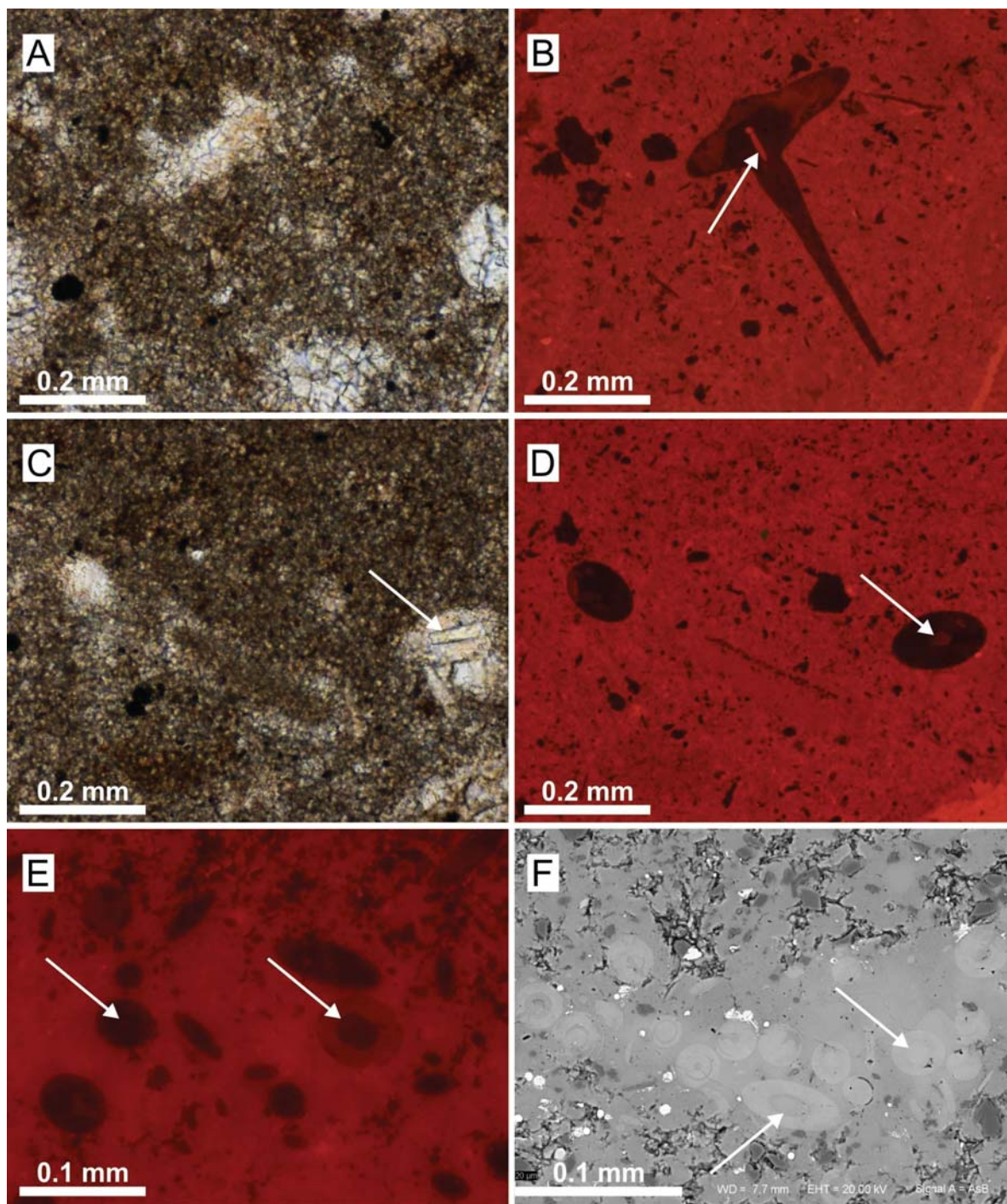
Text-fig. 4. Composition and texture of the mudstones. A-D – Paired microphotographs of plane polarized (PPL; A and C) and cathodoluminescence (CL; B and D) images. Mudstone in A and B (K01) exhibits thin lamination, whereas that in C and D (Sy5) has a massive texture. Blue, yellow, purple and green CL is related to siliciclastic material. Carbonates exhibit orange, red or dull CL. Note zoned dolomite crystals (Dol) and slightly flattened and corroded calcite-filled (Cal) microfossils; E – BSE image of two calcite-filled flattened microfossils surrounded by fine-grained siliciclastic material in Do3; F – CL image of a deformed and corroded calcitic macrofossil, supposedly a trilobite (red) in Sy3



Text-fig. 5. Comparison of carbonate material in mudstones and concretions. A-B – CL images of the same kind of a spherical microfossil that is not deformed in concretion Do2 (B), whereas compactionally flattened and corroded in the surrounding mudstone Do2m (A). Both microfossils are filled with calcite cement that has orange CL in the concretion, whereas dull CL in the mudstone; C-D – Paired microphotographs (PPL in C and CL in D) of a transition zone between a concretion Do3 (right) and a mudstone (left). The concretionary microspar exhibits much brighter CL (orange to red) than that of carbonate cements in the mudstone (dull). Note a bivalve shell replaced and filled by calcite with dull CL (arrow). E-F – BSE images revealing micromorphology of the concretionary microspar. Siliciclastic material (dark grey) and framboidal pyrite (white) are dispersed between anhedral microspar calcite (light grey). Note clay minerals clustered in the spaces between adjoining calcite crystals in F. Abbreviations used: Cal – calcite, Dol – dolomite, Py – pyrite, Qtz – quartz, Kfs – K feldspar, cm – clay minerals



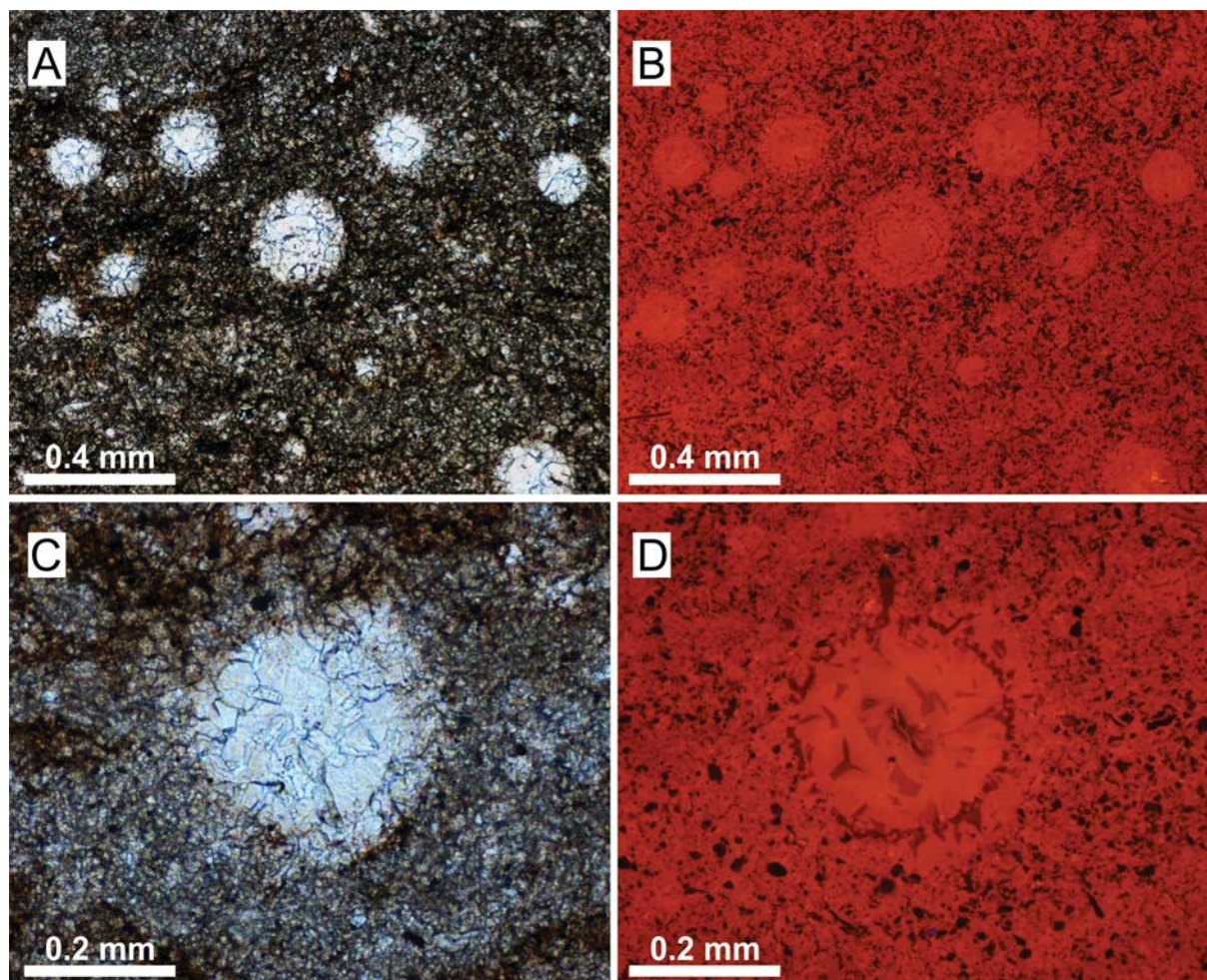
Text-fig. 6. 3-D preservation of benthic macrofossils in concretions observed in PPL (A, D, G), CL (B, E, H) and BSE (C, F, I). Shell material appears to be at least partly replaced. The surrounding matrix is composed of detrital material (mostly non-luminescent in CL and dark grey in BSE) cemented with microspar (orange to dull in CL, light grey in BSE). Note variable sizes of pyrite framboids (white in BSE). Complete bivalve in Sy1 (A-C), gastropod in Do4 (D-F) and brachiopod shells in Sy5 (G-I) are mainly filled with calcite cement; gastropod shell contains some detrital material supposedly near the aperture. Many shells enclose framboidal pyrites stuck to their inner surfaces (arrows in G-I)



Text-fig. 7. Calcified sponge spicules in concretions observed in PPL (A and C), CL (B, D, E) and BSE (F). Spicules are rarely visible in transmitted light, but become very clear in CL, as they exhibit mostly dull luminescence, that is in contrast with the concretionary microspar (orange). The dull luminescence of spicules corresponds to increased Fe contents manifested by light grey color in BSE (F). Arrows indicate location of the central voids. Concretions Sy1 (A-D) and Bo3 (E and F)

Nonetheless, original sedimentary fabrics, e.g. lamination or micronodular texture related to the abun-

dance of pellets, are preserved. Pyrite is developed as framboids dispersed between calcite crystals (Text-



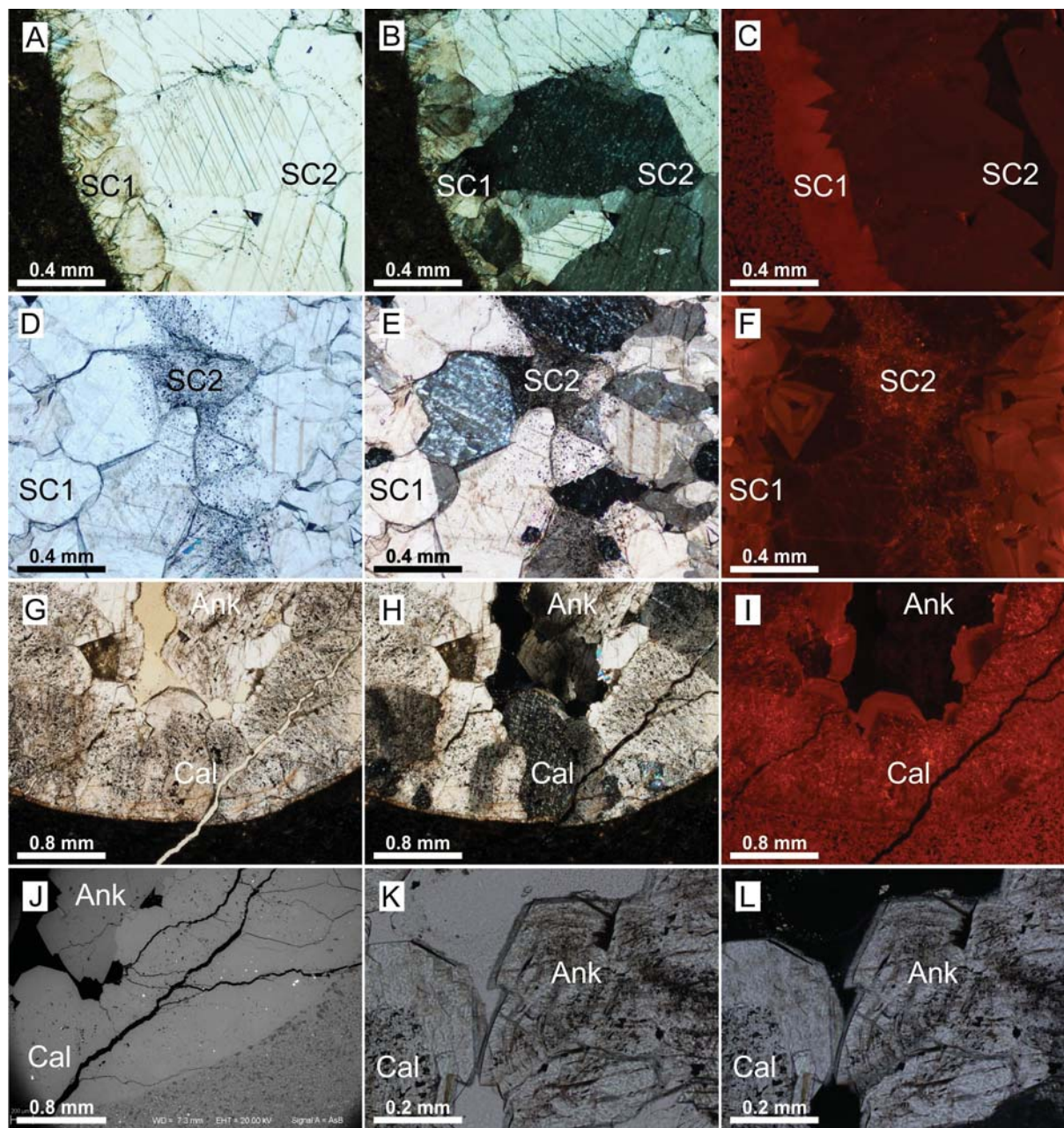
Text-fig. 8. Paired microphotographs (PPL and CL) of spherical microfossils (calcified radiolarian? tests) filled with calcite cement having variable, but mostly intensive orange CL in Bo1 (A-B) and Wy2 (C-D)

figs 6C, F, I and 7F) with the same sizes as those in the mudstones, but also as cubic crystals.

There is a major difference in the fossil content between the concretions and mudstones. The concretions are often full of complete and undeformed, although recrystallized, skeletal fossils composed of low-Mg calcite, e.g. mollusks (bivalves, gastropods, nautiloids), brachiopods (Text-fig. 6) and sponge spicules (Text-fig. 7), which do not occur in the surrounding mudstones. In transmitted light, identification of skeletal fossils is difficult, as the shells are recrystallized, filled with and surrounded by calcite cement. Shell morphology becomes clearer in CL and even very delicate skeletal structures were observed. Calcified microfossils (e.g. originally siliceous radiolarian tests) are the most common biogenic components in concretions from both basins (Text-

fig. 8). There are, however, substantial differences in microfacies between the basins (Suppl. Table 2). Concretions from the Lublin Basin occasionally exhibit lamination, rarely show micronodular fabric and are dominated by benthic assemblages with rare radiolarian tests. Specimens with abundant benthic fauna lack lamination, except concretion Sy2, where reworked benthic fauna was deposited together with a storm deposit. Samples from the Baltic Basin always show lamination; samples from Borcz-1 and Wysin-1 wells exhibit micronodular fabric, are full of radiolarian shells and do not contain benthic fauna, whereas samples from Kochanowo-1 and Opalino-2 wells are not micronodular and contain scarce microfossils and small bivalve shells.

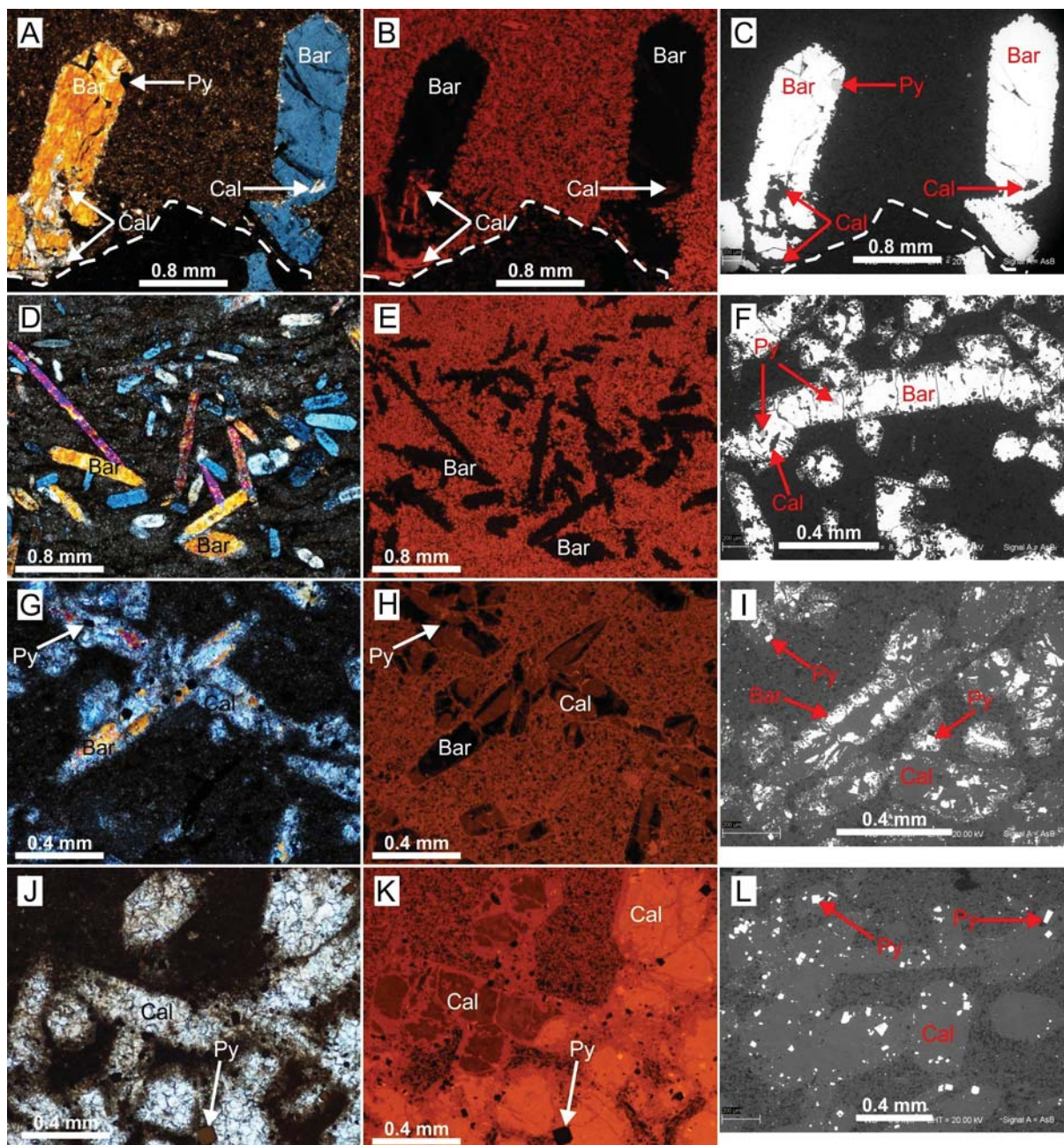
Mollusk and brachiopod shells are usually devoid of detrital material and the body chambers are filled



Text-fig. 9. Coarse-crystalline carbonate cements filling septarian cracks (A-F) and nautiloid shells (G-L). A-C – Two generations of septarian calcite in Do3: early SC1 (orange in CL) and late SC2 (dull to non-luminescent in CL). PPL, XPL and CL images, respectively; D-F – Inclusion-rich SC2 in Do1. PPL, XPL and CL images, respectively; G-J – Intrashell calcite (Cal) rich in bitumen inclusions and saddle ankerite (non-luminescent; Ank) filling a nautiloid shell in Sy2. PPL, XPL, CL and BSE images, respectively; K-L – Both saddle ankerite and calcite are inclusion-rich. PPL and XPL images, respectively

with sparite and pyrite framboids (Text-fig. 6). The shells show dull luminescence with some parts exhibiting similar orange luminescence to that of calcite cement suggesting replacement of original shell material. Calcified sponge spicules <0.1 mm in diameter

are often found in clusters (Text-fig. 7) and exhibit dull luminescence. All these skeletal elements are composed of calcite that exhibits uniform elemental compositions with <4 mol% of Mg, <0.5 mol% of Mn and ~1 mol% of Fe. This confirms that original



Text-fig. 10. Barite in the matrix of the concretions observed in cross-polarized (XPL) light (A, D, G), combined PPL and reflected light (J), CL (B, E, H, K) and BSE (C, F, I, L). Barite (Bar) exhibits vivid interference colors in XPL, white in BSE and is non-luminescent. The degree of replacement by calcite (Cal; orange and dull in CL, grey in BSE) increases from A-C to J-L. A-C – Insignificantly altered barite with small inclusions of calcite at the base of Sy4 concretion; D-F – Barite crystals with faces slightly corroded by concretionary calcite and inclusions of euhedral pyrite (Py) in Wyl; G-I – Significantly altered barite partly replaced by calcite associated with euhedral pyrite in Do4; J-L – Calcite pseudomorphs after barite (entirely leached) with abundant euhedral pyrite in Do3

skeletal carbonate underwent recrystallization. SEM-EDS analyses of the areas observed previously in CL show that Fe/Mn ratio controls the luminescence

of the skeletal calcite. Vivid and dull luminescence colors are related to moderate and high Fe/Mn ratios, respectively.

Microfossils are spherical features (~0.3 mm in diameter) that are replaced and filled with calcite with bright orange or dull luminescence, which contains ~2.2 mol% of Mg, <0.7 mol% of Mn and <0.9 mol% of Fe. They are not flattened and most of them probably represent calcified radiolarian tests (Text-fig. 8). Other rare fossils preserved in the concretions are trilobites, echinoderms and unidentified biogenic phosphates (Suppl. Table 2).

Apart from microcrystalline calcite, the concretions contain coarser-crystalline carbonate cements infilling shells and septarian cracks. The cross-cutting relationship between successive generations of septarian cements indicates two stages of cracking. The first septarian calcite (SC1) occurs only in the older generation of septarian cracks and exhibits orange luminescence (Text-fig. 9A–C). The second septarian calcite (SC2) lines the walls of the younger generation of cracks and may also fill the central parts of the older one. It is sometimes associated with euhedral pyrite. SC2 shows variable, but generally weak luminescence (mostly dull, but may grade to non-luminescent) and commonly contains numerous organic inclusions, supposedly bitumen (Text-fig. 9D–F). The elemental composition of septarian calcites changes from SC1 to SC2 towards lower Mg (from ~2.7 to ~2.4 mol%) and Mn contents (from ~0.6 to ~0.4 mol%), whereas Fe content increases (from ~0.1 to ~0.6 mol%). Very coarse-crystalline (even several centimeters), white, translucent barite is the last cement generation in the younger cracks (Text-fig. 3E).

Intrashell calcite exhibits variable elemental composition (Mg <5.6 mol%, Mn <0.6 mol% and Fe <1.8 mol%) and is usually orange to red in CL, but can change to dull or dark orange even within a single shell (Text-figs 6 and 8). This cement has, however, different elemental composition (relatively depleted in Mg and Fe and enriched in Mn) from analogous cement filling microfossils in the mudstones (Text-fig. 5A and B). Intrashell calcite is rarely followed by non-luminescent saddle ankerite (defined as dolomite with Fe content >10 mol%). Both cements are, in some cases, rich in bitumen inclusions (Text-fig. 9G–L).

White, euhedral, prismatic hexagonal barite crystals are found in clusters along some laminae, where they form even 10 mm long crystals (Text-fig. 10A–F). Alternatively, barite occurs as smaller (<1 mm long) crystals in oval domains in the center of some concretions (Text-figs 3D, 10G–L). Barite crystals are sometimes intergrown with each other forming rosettes (Text-fig. 10G–I). Barite does not exhibit luminescence and is replaced by calcite and euhedral pyrite (Text-fig. 10). Euhedral, cubic pyrite is espe-

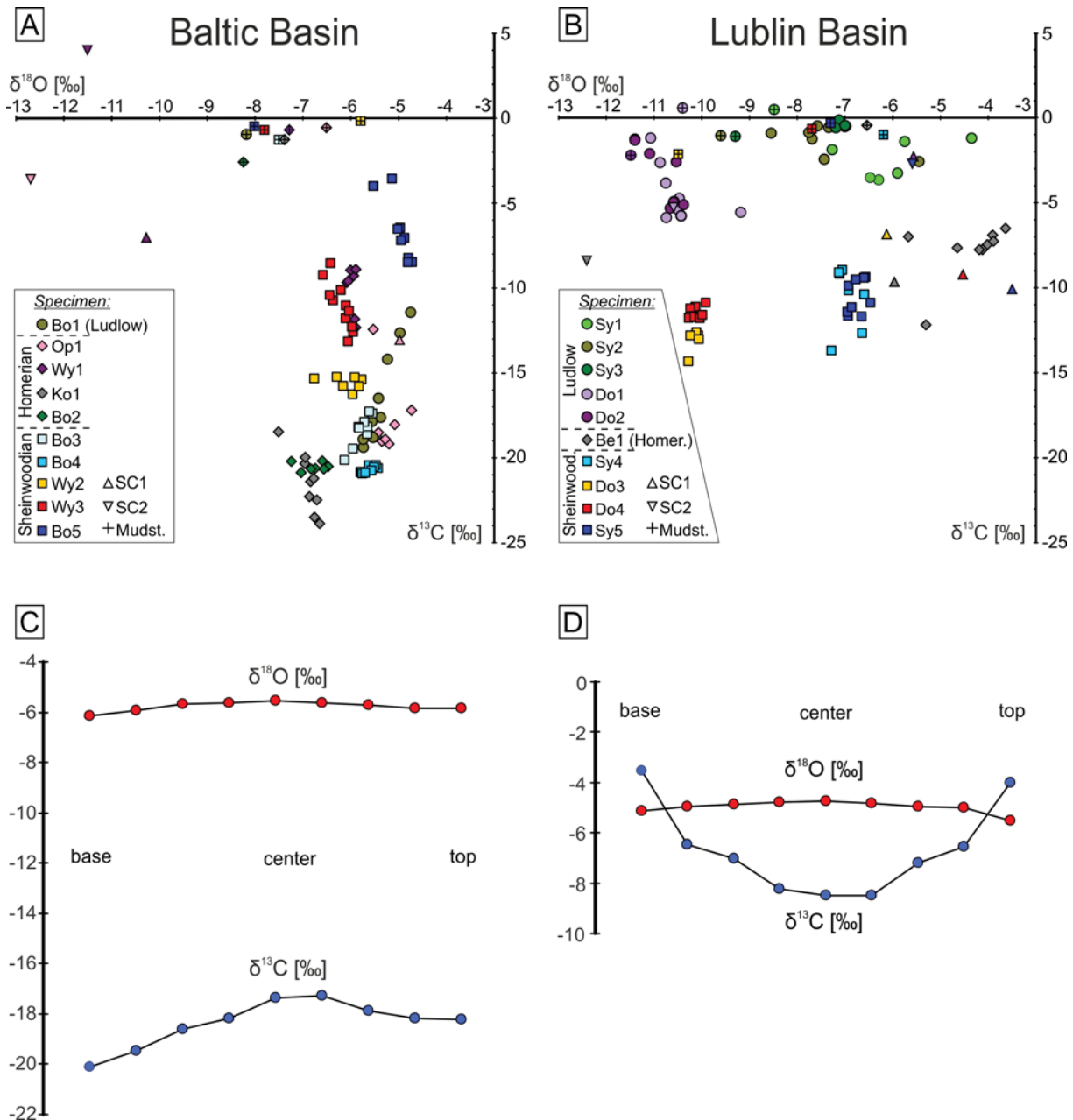
cially abundant in former barite crystals that were entirely replaced (Text-fig. 10J–L). The replacive calcite exhibits strongly variable luminescence even within a single barite crystal (Text-fig. 10H, K).

### Isotopic compositions

Results of isotopic measurements are given in Suppl. Table 4. The  $\delta^{13}\text{C}_{\text{org}}$  values of mudstones range between -31.6‰ and -27.6‰ ( $n = 19$ ) being related to the stratigraphic position and paleogeographic location of the samples. The  $\delta^{13}\text{C}_{\text{org}}$  values of the Sheinwoodian in the Baltic Basin are higher (from -30.1‰ to -27.6‰; average of -28.8‰;  $sd = 1.1$ ;  $n = 4$ ) than coeval ones in the Lublin Basin (from -31.5‰ to -30.6‰; average of -31.0‰;  $sd = 0.4$ ;  $n = 4$ ) and those of the Homerian in the Baltic (from -31.6‰ to -29.3‰; average of -30.2‰;  $sd = 1.1$ ;  $n = 4$ ) and Lublin (-29.0‰) basins. The  $\delta^{13}\text{C}_{\text{org}}$  values of the Ludlow samples are very stable and fall within a narrow range between -30.3‰ and -30.1‰ ( $n = 6$ ). One concretion sample (Sheinwoodian, Baltic Basin) yielded the highest  $\delta^{13}\text{C}_{\text{org}}$  value of -27.3‰.

The  $\delta^{13}\text{C}_{\text{carb}}$  values of samples collected from microcrystalline concretion matrix are negative and range from -23.9‰ to -0.1‰ (Text-fig. 11A and B). Concretions from the Baltic Basin exhibit overall lower  $\delta^{13}\text{C}_{\text{carb}}$  values (between -23.9‰ and -3.6‰; mean -15.7‰) than those from the Lublin Basin (between -14.3‰ and -0.1‰; mean -6.7‰). A trend of increasing  $\delta^{13}\text{C}_{\text{carb}}$  values from the Sheinwoodian (<-9‰) to the Ludfordian (>-6‰) occurs in the Lublin Basin, but is not observed in the Baltic Basin, which precludes a stratigraphic control on  $\delta^{13}\text{C}_{\text{carb}}$ . The  $\delta^{18}\text{O}_{\text{carb}}$  values of samples collected from concretion matrix are negative and range from -11.4‰ to -3.6‰ (Text-fig. 11A and B). However, the range becomes narrower (between -8.5‰ and -3.6‰), but still wider than that of the Lublin Basin, when the very low and uniform  $\delta^{18}\text{O}_{\text{carb}}$  values (around -11‰) from Dobryniów OU-1 well are excluded.

The  $\delta^{13}\text{C}_{\text{carb}}$  and  $\delta^{18}\text{O}_{\text{carb}}$  values differ between concretions. Within individual specimens,  $\delta^{18}\text{O}_{\text{carb}}$  values are rather uniform (spread is <2‰), whereas  $\delta^{13}\text{C}_{\text{carb}}$  differ by <8‰. Thirteen concretions exhibit rather small isotopic variability. Isotopic compositions of the other seven concretions show a covariance between  $\delta^{13}\text{C}_{\text{carb}}$  and  $\delta^{18}\text{O}_{\text{carb}}$  values. Positive correlation ( $r > 0.65$ ), is observed for Bo1, Bo3 and Bo4, whereas negative correlation ( $r < -0.65$ ) is observed for Bo5, Do2, Kol and Wy3 concretions (Text-fig. 11). The  $\delta^{18}\text{O}_{\text{carb}}$  values decrease from the center to the edge of these concretions, so the positive and



Text-fig. 11. A-B – Plots of  $\delta^{13}\text{C}_{\text{carb}}$  vs.  $\delta^{18}\text{O}_{\text{carb}}$  of all samples from the Baltic (A) and Lublin Basins (B). Shapes of projection points for concretion matrix and mudstone samples indicate their stratigraphic position: squares – Sheinwoodian, diamonds – Homerian, circles – Ludlow, whilst colors indicate specimens. Triangles represent septarian calcites; C-D –  $\delta^{13}\text{C}_{\text{carb}}$  and  $\delta^{18}\text{O}_{\text{carb}}$  values along vertical transects across concretions Bo3 (C) and Bo5 (D) that exemplify isotopic trends towards lighter and heavier  $\delta^{13}\text{C}_{\text{carb}}$  values from the centers to the edges, respectively. Note rather uniform  $\delta^{18}\text{O}_{\text{carb}}$  values

negative correlations are associated with decreasing and increasing  $\delta^{13}\text{C}_{\text{carb}}$  values in the same direction, respectively (Text-fig. 11C and D). The  $\delta^{13}\text{C}_{\text{carb}}$  values of the mudstones vary between  $-2.7\text{‰}$  and  $+0.6\text{‰}$ , whereas  $\delta^{18}\text{O}_{\text{carb}}$  values can be very different,

ranging from  $-11.5\text{‰}$  to  $-5.8\text{‰}$  (Text-fig. 11A and B). The lowest  $\delta^{18}\text{O}_{\text{carb}}$  values ( $<-10\text{‰}$ ) were measured in samples from the Dobryniów OU-1 well. Dolomite/calcite ratio in the mudstones (up to 3; Suppl. Table 1) is related neither to  $\delta^{13}\text{C}_{\text{carb}}$ , nor  $\delta^{18}\text{O}_{\text{carb}}$  values. All

mudstones (except Do4m) exhibit similar or lower  $\delta^{18}\text{O}_{\text{carb}}$  values than those of the associated concretions. The  $\delta^{13}\text{C}_{\text{carb}}$  values of the septarian cements are similar to or higher, even by over 20‰, than those of the concretion matrix (Text-fig. 11A and B). The  $\delta^{18}\text{O}_{\text{carb}}$  values of the septarian cements can be similar to or diverge in both directions from those of the concretion matrix. SC2 always exhibits higher  $\delta^{13}\text{C}_{\text{carb}}$  and lower  $\delta^{18}\text{O}_{\text{carb}}$  values than those of SC1. Isotopic composition of SC1 ranges from -13.1‰ to -2.2‰ for  $\delta^{13}\text{C}_{\text{carb}}$  and from -6.2‰ to -3.5‰ for  $\delta^{18}\text{O}_{\text{carb}}$  (with one exception of -10.2‰). SC2 has  $\delta^{13}\text{C}_{\text{carb}}$  values between -8.5‰ and +4.1‰ and  $\delta^{18}\text{O}_{\text{carb}}$  values between -12.7‰ and -10.6‰ (with one exception of -5.6‰).

The S and O isotope compositions of septarian barites in concretions Sy5 and Wy2 are different (Suppl. Table 4). The  $\delta^{34}\text{S}_{\text{sulf}}$  and  $\delta^{18}\text{O}_{\text{sulf}}$  values of Sy5s3 are higher (+43‰ and +17‰, respectively) than those of Wy2s (+14‰ and +14‰), respectively. The  $\delta^{18}\text{O}_{\text{sulf}}$  values of these septarian barite crystals are within the 95% confidence interval of contemporaneous seawater sulfate (+12‰ to +17‰; Claypool *et al.* 1980). Yet, Wy2s exhibits depleted S isotope composition, whereas Sy5s3 is strongly enriched in  $^{34}\text{S}$  relative to the mean  $\delta^{34}\text{S}_{\text{sulf}}$  value of contemporaneous seawater (+23‰ to +28‰, Paytan *et al.* 2011; Strauss 1997). Three barite crystals occurring in the matrix of concretions Sy4 and Sy5 are enriched in  $^{34}\text{S}$  as well, as their  $\delta^{34}\text{S}_{\text{sulf}}$  values range from +37‰ to +64‰. Both barite types (in matrix and septarian cracks), in concretion Sy5 exhibit similar  $\delta^{34}\text{S}_{\text{sulf}}$  values (+44‰ and +43‰, respectively).

## DISCUSSION

### Timing and diagenetic setting of concretionary growth

The concretions must have at least started to form shortly after deposition, close to the sediment-water interface and prior to significant mechanical compaction of the sediments, which is indicated by the following facts:

(1) Lamination is mostly perfectly horizontal throughout each concretion, whereas lamination in the surrounding mudstones is warped around the concretions. Only three specimens exhibit insignificant inclination of laminae in their outer parts, but their angles (<15°) are far lower than those of the surrounding mudstones (<45°). Moreover, laminae in concretions are 2 to 3 times thicker than in the associated mudstones.

(2) Carbonate skeletal elements of fossil fauna have been preferentially preserved in the concretions, although they underwent recrystallization. The spherical microfossils and macrofossils bear no sign of any compactional flattening and are often complete in the concretions. For instance, bivalve and brachiopod shells are usually composed of both valves in their primary positions. In contrast, microfossils in the surrounding mudstones, if preserved, are always flattened (cf. Blome and Albert 1985; Bojanowski *et al.* 2014), whereas macrofossils were mostly dissolved.

(3) Concretionary calcite is very abundant (about 80%) in the concretions. It forms a continuous framework, in which the detrital grains are strongly dispersed indicating that porosity was very high and detrital material not yet lithified during calcite precipitation (cf. Morad and Eshete 1990; Mozley 1996; Raiswell and Fisher 2000; Sellés-Martinez 1996). It is also possible that this early cement precipitation was able to displace the detrital grains. Later-stage replacive calcite also contributed to the high carbonate content.

(4) Increasing compaction causes reorientation of platy minerals, which drives progressive anisotropy of permeability in fine-grained sediments (Bennett *et al.* 1991). When concretions form in semi-compacted sediments, they acquire lenticular morphologies (Sellés-Martinez 1996). As most of the concretions examined are subspherical, permeability and, therefore, diffusivity of the surrounding sediments must have been almost isotropic during their growth.

This early diagenetic calcite precipitation must have at least started in the uppermost several centimeters or decimeters of sediments forming a compaction-resistant framework (cf. Wetzel 1992; Mozley 1996) sheltering original textures, faunal assemblages and early-diagenetic barites from deformation and dissolution. The cement content was still low, as otherwise preferential deflection of the underlying laminae under the load of a fully cemented concretion would be expected.

### Paragenetic sequence and sources of substrates for non-concretionary mineral phases

The order of precipitation of authigenic phases was determined on the basis of their micromorphology, elemental composition, cathodoluminescence and mutual textural relationships. Framboidal pyrite and barite (except the septarian variety), presumably also dolomite, formed prior to or partly during the early stages of concretionary growth, so they represent early-diagenetic precipitates. The different, but

mostly small sizes of pyrite framboids indicate that they could have started to form already in the water column, but their growth continued below the seafloor as well, where they attained larger sizes (Wignall and Newton 1998; Wilkin *et al.* 1996). Therefore, framboidal pyrite formed as the first authigenic mineral uniformly throughout freshly deposited sediments in the bacterial sulfate reduction (BSR) zone (cf. Coleman and Raiswell 1993; Peckmann and Thiel 2004).

Authigenic barite in marine sediments can have a biogenic, diagenetic or hydrothermal origin (Torres *et al.* 1996). The large size and euhedral habit of these barite crystals exclude biogenic formation as such a biogenic origin is ascribed only to oval grains about 1  $\mu\text{m}$  in diameter (Dehairs *et al.* 1980; Bishop 1984; see Paytan *et al.* 2002 for a review). S isotope analyses are a means of deciphering the genesis of barite between hydrothermal and diagenetic (Paytan *et al.* 2002). The  $\delta^{34}\text{S}$  values of early barite occurring as large crystals in the concretion matrix are well above the sulfur isotope composition of the Late Silurian seawater sulfate. Such a strong  $^{34}\text{S}$  enrichment can only be explained by microbial reduction of sulfate dissolved in pore water in a semi-closed diagenetic environment, when sulfate became already significantly depleted (Bréhéret and Brumsack 2000; Riedinger *et al.* 2006). Bacteria preferentially utilize sulfate with  $^{32}\text{S}$  causing residual enrichment of  $^{34}\text{S}$  in the remaining sulfate pool in such settings (Canfield 2001). Therefore, barite occurring in the concretionary matrix is early-diagenetic and precipitated in the BSR zone, but deeper than framboidal pyrite, where marine sulfate was already strongly used up. The source of  $\text{Ba}^{2+}$  was probably dissolution of biogenic barite particles that were deposited on the seafloor, but buried to the sulfate-free diagenetic zone extending below (Torres *et al.* 1996).  $\text{Ba}^{2+}$  released into the pore water migrated upwards (Riedinger *et al.* 2006) and when it reached the sulfate-bearing zone, barite precipitated as euhedral, large crystals. Dolomite precipitated at the base of the BSR zone where sulfate became significantly depleted or in deeper diagenetic zones (cf. Hennesy and Knauth 1985; Compton 1988), as sulfate ions are effective inhibitors for dolomite formation (Baker and Kastner 1981). Thus, a late diagenetic formation post-dating concretionary growth may not be ruled out.

The concretions grew through gradual precipitation of microspar calcite. The concretionary growth was associated with replacement of shells and barite crystals in the concretions. At some point, the first set of septarian cracks opened and was subsequently filled with early septarian calcite (SC1). The second

set of septarian cracks opened after precipitation of SC1 and was filled with late septarian calcite (SC2) followed by septarian barite. Late carbonate cements (calcite and saddle ankerite), often with bitumen inclusions, precipitated within large shells in the concretions as well.

It is difficult to constrain the time relations between the diagenetic processes taking place within the concretions and in the surrounding mudstones. Framboidal pyrite, barite and dolomite surely precipitated in the mudstones. The silt-sized carbonate grains in the mudstones are difficult to interpret. Their morphology is mostly not indicative of their origin. The high Mg and low Mn contents along with  $\delta^{13}\text{C}_{\text{carb}}$  and  $\delta^{18}\text{O}_{\text{carb}}$  values being close to those of contemporaneous seawater (Azmy *et al.* 1998), suggest that these grains may represent either intraclasts, very early seawater-derived cements, cements precipitated from dissolution of primary carbonates, or recrystallized micrite. It is clear that both dissolution and precipitation of carbonates did take place after deposition. The microspar calcite cement observed in some mudstones exhibits contrasting properties to those of concretionary microspar and can be related to later diagenetic stages, as suggested by its very high Fe/Mn ratio (cf. Curtis and Coleman 1986). Thus, we assume that at least some part of the silt-sized calcite formed by late-diagenetic recrystallization or reprecipitation after dissolution of primary marine carbonate grains. Yet, some calcitic grains in the mudstones may be intraclasts, which were more resistant to dissolution than biogenic or micritic grains that were likely composed of metastable high-Mg calcite or aragonite (e.g. gastropod shells).

#### Sources of substrates for concretionary calcite

Stable C and O isotope compositions of carbonate material are used to reconstruct the sources of inorganic carbon dissolved in parent pore water (DIC – *dissolved inorganic carbon*) and to investigate the sources of pore water and temperature variations during calcite precipitation at shallow burial provided that original isotopic ratios are preserved. Although carbonate shells underwent secondary alteration (including neomorphism), the concretionary microspar cement was not recrystallized, as this would have modified its original development, most of all by increasing crystal size (Morse and Casey 1988) and transforming its micromorphology (Saigal and Bjørlykke 1987; Bojanowski *et al.* 2014), which is not the case. Oxygen isotopes are vulnerable to secondary alteration, especially at increased temperatures,

which may reset the isotopic ratios by re-equilibration between the brines and carbonate material. Resetting of oxygen isotopic ratios at increased temperature results in depletion of  $^{18}\text{O}$  and in unification of  $\delta^{18}\text{O}_{\text{carb}}$  values of calcite concretions (Dix and Mullins 1987; Bojanowski *et al.* 2014). Although the concretions examined exhibit a narrow range of  $\delta^{18}\text{O}_{\text{carb}}$  values within individual specimens ( $<2\text{‰}$ ; Text-fig. 11A and B), their  $\delta^{18}\text{O}_{\text{carb}}$  values (mean values between  $-7.4\text{‰}$  and  $-4.4\text{‰}$ ) are within or slightly lower than the range of the Silurian seawater ( $-6\text{‰}$  to  $-4\text{‰}$ ; Azmy *et al.* 1998), which suggests that the original isotopic composition was preserved, as early-diagenetic cements are expected to precipitate at a slightly higher temperature than that of bottom water. Only the concretions from the Dobryniów OU-1 well are strongly depleted in  $^{18}\text{O}$  and their  $\delta^{18}\text{O}$  values vary by less than  $1\text{‰}$  within a single concretion, which points to reequilibration of O isotope ratios at an elevated temperature. This O isotope resetting was probably caused by an abnormally high temperature related to maximum burial in this area, as exceptionally high maturity of organic matter  $\sim 3\%$  Ro was recorded in the Silurian deposits in Łopiennik IG-1 well (Grotek 2009) that is located several kilometers away from the Dobryniów OU-1 well.

The amount of carbonate material inherited from the sediments is insignificant in the concretions. Therefore, their bulk isotopic composition is chiefly controlled by the isotopic composition of concretionary cements with minor influence from sedimentary and biogenic carbonates with  $\delta^{13}\text{C}_{\text{carb}}$  values around  $0\text{‰}$ , as represented by mudstone samples. The negative  $\delta^{13}\text{C}_{\text{carb}}$  values of the concretion matrix indicate that the main source of DIC was microbial oxidation of organic matter (OM) during early diagenesis (Irwin *et al.* 1977; Curtis and Coleman 1986), which transfers organic carbon to DIC without a significant change in the C isotope composition (Cody *et al.* 1999). Formation of framboidal pyrite predating concretionary growth was related to BSR (see above), so the negative  $\delta^{13}\text{C}_{\text{carb}}$  values of the concretions can only be linked to BSR as the main DIC source, as fermentation is related to fractionation of C isotopes in the opposite direction. The C isotope composition of OM in the associated mudstones (between  $-32\text{‰}$  and  $-28\text{‰}$ ) provides a rough estimation of the composition of the organic source for the concretions. The original  $\delta^{13}\text{C}_{\text{org}}$  values of OM deposited on the basin floor were probably slightly higher, e.g. up to  $-25\text{‰}$ , as post-depositional alteration of OM leads to preferential preservation of  $^{13}\text{C}$ -depleted compounds (Lehmann *et al.* 2002). Thus, the lowest  $\delta^{13}\text{C}_{\text{carb}}$  values of con-

cretions (between  $-24\text{‰}$  and  $-10\text{‰}$ ) must be associated with the domination of BSR-derived DIC during precipitation of concretionary microspar. The role of BSR-derived DIC diminishes towards higher values (between  $-10\text{‰}$  and  $0\text{‰}$ ), for which another, “heavier” DIC source (relatively enriched in  $^{13}\text{C}$ ) must have been also significant. The concretions formed at least partly by an outward growth (see below), so the tendency of decreasing  $\delta^{18}\text{O}_{\text{carb}}$  values towards their margins suggests that they grew during a period of decreasing O isotope ratio, probably driven by a slight increase of temperature during gradual burial. Therefore, concretions with positive correlations between  $\delta^{13}\text{C}_{\text{carb}}$  and  $\delta^{18}\text{O}_{\text{carb}}$  values grew when the role of the “heavier” DIC source, which was most likely seawater or dissolution of primary carbonate grains, was decreasing. Consequently, concretions with negative correlations grew when the role of the “heavier” DIC source, which was probably methanogenesis (Me; Irwin *et al.* 1977; Curtis and Coleman 1986) or dissolution of carbonate grains, was increasing. Concretions without correlation between  $\delta^{13}\text{C}_{\text{carb}}$  and  $\delta^{18}\text{O}_{\text{carb}}$  values have not experienced changes either in the sources of DIC or temperature while forming, probably because they were formed in a very stable diagenetic conditions in the BSR zone or over a relatively short period.

The septarian cements represent individual cement generations that can be sampled separately, not a mixture of several generations of microcrystalline cements and sedimentary carbonates, as is the situation in the concretionary matrix. The isotopic composition of a septarian cement provides, therefore, a precise characterization of a particular event in the diagenetic history. The  $\delta^{18}\text{O}_{\text{carb}}$  values of the early septarian calcite (SC1) are mostly within the range typical for contemporaneous seawater and similar to those of the concretionary matrix. This means that SC1 precipitated at similar shallow depths as concretionary microspar. Some SC1 exhibit  $\delta^{18}\text{O}_{\text{carb}}$  values that are in fact higher than those of associated concretions. This can be tentatively explained by a prolonged precipitation of concretionary microspar and partly pervasive concretionary growth (see below), which resulted in the bulk  $\delta^{18}\text{O}_{\text{carb}}$  values of the concretion body being buffered between those of early (roughly represented by  $\delta^{18}\text{O}_{\text{carb}}$  of SC1) and late microspar generations (with  $\delta^{18}\text{O}_{\text{carb}}$  values lower than those of SC1). The fairly negative  $\delta^{13}\text{C}_{\text{carb}}$  values ( $\sim -10\text{‰}$ ) of SC1 are similar to those of the concretionary matrix, which confirms that the DIC pool was composed of a mixture of BSR-derived and a “heavier” DIC (marine DIC, liberated from dissolution of carbonates or related to Me) during the early-concretionary stage.

The late generation of septarian calcite (SC2) is enriched in Mn, Fe,  $^{13}\text{C}$  and depleted in  $^{18}\text{O}$  relative to SC1. This indicates that SC2 precipitated in a deeper diagenetic environment, in more reducing conditions and at an elevated temperature (Curtis and Coleman 1986). The highest  $\delta^{13}\text{C}_{\text{carb}}$  value (+4.1‰) noted for SC2 clearly shows that an additional source of DIC with very high  $\delta^{13}\text{C}_{\text{carb}}$  values appeared, which was enriched in  $^{13}\text{C}$  relative to marine DIC or that liberated by dissolution of carbonates. Potential sources of  $^{13}\text{C}$ -enriched DIC include Me (Irwin *et al.* 1977) or thermal decarboxylation (De) of already strongly degraded and isotopically fractionated kerogen (Galimov 1980; Whiticar *et al.* 1986). The  $\delta^{13}\text{C}_{\text{carb}}$  values of the rest of the SC2 samples range from -8.5‰ to -1.2‰, which may also be related to DIC liberated by Me or De, but compromised by an addition of DIC from dissolution of carbonates. Me usually operates at temperatures <75°C (Wiese and Kvenvolden 1993), whereas De operates at >50°C (Peters *et al.* 2005), so both processes are likely, as these temperature ranges can be reconciled with the very low  $\delta^{18}\text{O}_{\text{carb}}$  values of these samples and the thermal history of the host rocks.

Barite occurs in the concretions and was not found in the surrounding mudstones, although large barite crystals were observed in mudstones of the Pelplin Fm in other wells. Barite is relatively insoluble mineral, but it is prone to dissolution during deep burial where sulfate becomes exhausted in pore water (Torres *et al.* 1996; Riedinger *et al.* 2006) and can survive only if favorable conditions occur. Early barite is commonly corroded or even pseudomorphed by calcite in the concretions. The degree of replacement by calcite depends on the location within concretions. Barite domains contain some unaltered barite only when they are enveloped by large concretions. Moreover, barites occurring in concretions along horizontal planes do not extend beyond the concretions. Therefore, barite was clearly more effectively isolated from the sulfate-free pore water by the microcrystalline concretion body, whereas it was entirely leached in the surrounding sediments. Euhedral pyrite, which is preferentially associated with strongly altered barite crystals, must have formed as a consequence of barite replacement, as considerable quantity of sulfate was liberated from dissolution of barite and subsequently reduced to precipitate pyrite. This pyrite is also associated with SC2 that predates septarian barite. Thus, sulfate-free conditions leading to barite dissolution occurred after SC1 and continued during precipitation of SC2, which must have taken place in the Me and/or De zones.

Septarian barite bears no sign of dissolution, which suggests that it formed after the early-diagenetic barite crystals and when favorable conditions were reestablished. In concretion Sy5, the S isotope composition of septarian barite is similar to that of early-diagenetic barite and SC2 is associated with euhedral pyrite, which suggests that substrates for septarian barite could have been derived from dissolution of the early-diagenetic barite. The  $\delta^{34}\text{S}$  value of septarian barite in Wy2 is by 9–14‰ lower than that of the Late Silurian seawater sulfate. This may be related either to oxidation of hydrothermal  $\text{H}_2\text{S}$  (Paytan *et al.* 2002) or oxidation of microbially formed sulfides that are depleted in  $^{34}\text{S}$ , e.g. framboidal pyrite (Bottrel *et al.* 2000; Raiswell *et al.* 2002). Moreover, euhedral pyrite was not detected in this concretion, which suggests that precipitation of septarian barite was not always related to dissolution of early-diagenetic barite.

Saddle ankerite is the last carbonate cement observed in the rocks examined. Formation of saddle dolomites and ankerites is linked to precipitation from hot basinal fluids at temperatures >100°C and typically at least coinciding with the “oil window” (Al-Aasm 2003; Davies and Smith 2006). The Wenlock–Ludlow series experienced maximum burial in the Late Carboniferous, when they went through the “oil window” and reached the “dry gas window” conditions (Botor *et al.* 2017). Both saddle ankerite and the preceding late calcite cements contain bitumen inclusions, which can tentatively be linked to petroleum generation and migration (Sirat *et al.* 2016).

The  $\delta^{13}\text{C}_{\text{carb}}$  values of the mudstones examined are always lower than that of Silurian marine DIC (~+2‰; Prokoph *et al.* 2008), which can be explained by the addition of authigenic carbonates (mostly dolomite). The most depleted  $\delta^{13}\text{C}_{\text{carb}}$  values of mudstones are lower by ~4‰ than those of marine DIC, which is the case for Do3m sample that is especially rich in a late Fe-rich calcite cement. This indicates that authigenic carbonates in mudstones exhibit slightly negative  $\delta^{13}\text{C}_{\text{carb}}$  values, which may be attributed to BSR-derived or De-derived DIC for early and late carbonate cements, respectively. It is evident that the mudstones experienced dissolution of biogenic carbonates between these cementation events.

### Concretionary growth mechanism

The lack of concentric zoning, plane-parallel lamination throughout the entire concretions, as well as uniform content, micromorphology and the elemental composition of concretionary cement from center to edge of the concretions may be indicative of a per-

vasive mode of concretionary growth (Mozley 1996; Raiswell and Fisher 2000). Concretions formed in that way grow by simultaneous precipitation of microcrystalline cement within the entire space of the future concretion. However, there is also evidence of a concentric outward growth of the concretions examined. Inclination of laminae in some specimens indicates that their outer parts were cemented by concretionary calcite at a slightly later stage than their central parts. This late stage of concretionary growth added already slightly deflected laminae around the initial concretion. Still, this stage took place in only slightly compacted sediments, as the inclination of the laminae in the outer parts of the concretions is much lower ( $<15^\circ$ ) than that of the surrounding, fully compacted mudstones ( $<45^\circ$ ). Therefore, the concretions were formed by a combination of pervasive and concentric growth mechanisms (e.g. Bojanowski and Clarkson 2012). Namely, at the stage of concretion enlargement cements were precipitated not only beyond (concentric end-member), but also within the limits of an existing concretion by occluding the intercrystalline pore space (pervasive end-member). Such complex growth mechanism makes interpretation of the bulk isotopic composition problematic, as powdered samples for isotope analyses comprise several cement generations. This may explain the relatively low spread of  $\delta^{13}\text{C}_{\text{carb}}$  and  $\delta^{18}\text{O}_{\text{carb}}$  values within individual concretions, which represent a mass balance between different DIC sources and precipitation temperatures for all cement generations present in each sample.

Inclination of laminae developed when the concentric mode prevailed during the gradual increase of the overburden causing compaction progress. Abundant carbonate precipitation in fine-grained sediments with low permeability requires even several thousands of years to form a concretion (e.g. Raiswell 1988; Coleman and Raiswell 1993). The calculated sedimentation rates for uncompacted mudstones give estimates between 4 and 9 cm/kyrs, which shows that a concretion formed over 5 thousand years would have been buried merely by 20–45 cm during its growth. This confirms that the concretionary growth was able to take place in a stable diagenetic environment, i.e. entirely within the BSR zone, and during an insignificant progress of compaction of the surrounding sediments.

### **Paleoenvironmental implications**

The mineral composition, high organic carbon content (median TOC contents in the Baltic and Lublin basins are 0.7 and 1.5%, respectively, with a maximum of 9.5%) and textural characteristics

(e.g. lamination, peloids, fine grain size, distribution of pyrite framboid diameters) of mudstones in the Pelplin Formation indicate that they were formed predominantly by hemipelagic settling albeit interrupted by periods of erosion and deposition from fast moving suspensions in suboxic to anoxic conditions (Kosakowski *et al.* 2015). Because carbonate fossils are rarely preserved in the mudstones, little is known about the paleoenvironmental conditions that occurred in both basins during the Wenlock and Ludlow. This work partly fills this gap, as diverse faunal assemblages and early-diagenetic barite have been preferentially preserved in the concretions and much information could be recovered.

The C isotope composition of the concretions provides evidence of a link between the accumulation and microbial degradation of a large amount of organic matter and carbonate precipitation in oxygen-free diagenetic conditions. The extent of this concretionary carbonate authigenesis in the Silurian organic carbon-rich mudstones is extraordinary and doubtlessly must be related to high organic input and the low rate of detrital accumulation. High marine productivity is confirmed by the abundance of planktic microfossils (e.g. radiolarian tests) and pellets, especially in the Baltic Basin. Early-diagenetic barite is also typically associated with areas of high marine primary productivity where deposition of organic carbon-rich sediments takes place (Dean *et al.* 1997; Dehairs *et al.* 1980; Paytan *et al.* 1996). The burial depth range which has favorable conditions for early-diagenetic barite precipitation is small, as it is limited to the deep parts of the BSR zone (Riedinger *et al.* 2006). Continuous deposition at a relatively stable pace would have caused a constant downward migration of the sediments through the sulfate-methane transition zone (SMTZ), which would not have allowed for abundant barite precipitation (Br  h  ret and Brumsack 2000). Therefore, favorable conditions for the growth of barite domains or accumulations of barite crystals along some layers must have developed during prolonged periods of deceleration or breaks in sediment accumulation. Mean sedimentation rates estimated for the Wenlock deposits in both basins are indeed low ( $<10$  mm/kyrs for uncompacted sediments). The resultant steady diagenetic conditions allowed abundant calcite and barite precipitation by the stabilization of the SMTZ at a certain depth for a longer time. Because concretions appear in great numbers in the Wenlock and Ludlow strata without gaps in both basins, which are about 500 km apart, the cause for such a slow sedimentation rate must have been at least regional. The extent

of conditions favorable for abundant early-diagenetic carbonate precipitation took place over an even larger area, as similar concretions to those examined in this study have been reported from the Silurian organic carbon-rich mudrocks in various parts of the East European Craton, e.g. Bornholm in Denmark (Buchardt and Nielsen 1985), central Sweden (Morad and Eshete 1990) and the Holy Cross Mountains in Poland (Malec *et al.* 2016). The concretions from Bornholm and Poland are of a Wenlock age, whereas the Swedish ones occur in the Llandovery series. The concretions exhibit similar stable C and O isotope compositions and petrographic properties, although those from Sweden are affected by strong recrystallization. What is particularly pinpointing is the presence of calcite pseudomorphs apparently replacing euhedral sulfate minerals that are associated with euhedral late pyrite (cf. fig. 5 in Morad and Eshete 1990 and fig. 18D in Malec *et al.* 2006), although the authors of the latter work proposed another explanation. These features are very similar to the former barite crystals replaced by calcite presented in this study (see Text-fig. 10).

Our data points to some differences in paleoecological conditions between the Baltic and Lublin basins (Table 1). The occurrence of nectic fauna and abundance of radiolarian tests, together with the absence of benthic fauna in the concretions indicate a more basinal setting with very high marine productivity in the Baltic Basin. On the other hand, the appreciable quantity of benthic shelly organisms together with the scarcity of radiolarian tests is consistent with offshore neritic depths and relatively lower productivity in the Lublin Basin. A deeper environment in the Baltic Basin is also indicated by the thin lamination and micromodular texture preserved in the concretions. Despite its greater depth, the Baltic Basin was closer to the detrital source, i.e. the Caledonian orogenic front to the west, which is manifested by the higher sedimentation rate and higher

quartz/clay ratio in the mudstones (Suppl. Table 1). The shallower setting in the Lublin Basin allowed for the occasional accumulation of storm deposits. The size distribution of framboidal pyrites is similar and indicates common redox conditions in both basins. Therefore, the abovementioned sedimentological differences cannot be explained by different redox conditions in the basins. The overall higher  $\delta^{13}\text{C}_{\text{carb}}$  values of concretions from the Lublin Basin than those from the Baltic Basin probably result from the abundance of macrofossils that contain late intrashell calcite with relatively heavy C isotope ratios and should not be interpreted in terms of paleoenvironmental differences.

The stable C and O isotope composition of the concretions indicates that Me and De operated in the Silurian deposits, which is in line with their high TOC content and indicates that biogenic methane and thermogenic hydrocarbons were produced during early and burial diagenesis, respectively. The occurrence of bitumen inclusions in the late carbonate cements, e.g. saddle ankerite, confirms that thermogenic hydrocarbons might have migrated through the Pelplin Fm. during deep burial stage.

## CONCLUSIONS

The concretions started to grow close to the sediment-water interface, prior to mechanical compaction. They formed by a combination of concentric and pervasive growth mechanisms. The initial stages of cementation produced a compaction-resistant framework, which protected the original sedimentary structures, faunal assemblages and early-diagenetic barite. The concretions formed mainly as a result of oxidation of organic matter coupled to bacterial sulfate reduction (BSR). Other possible sources of dissolved inorganic carbon (DIC) were seawater, dissolution of carbonate grains and methanogenesis

	Baltic Basin	Lublin Basin	Comments/Interpretation
accumulation rate in Wenlock	23–31 mm/kyrs	13 mm/kyrs	Baltic Basin closer to orogen
mineralogical composition	the same suite of minerals, but:		
quartz/2:1 layer phyll. in mudstones	from 1.2 to 3.0; mean 1.8	from 0.8 to 1.7; mean 1.2	higher rate of detrital input to the Baltic Basin
pellets	8/10 concretions	2/10 concretions	higher plankton productivity in the Baltic Basin
<i>Radiolaria</i>	8/10 concretions	2/10 concretions	
benthic fauna	2/10 concretions	9/10 concretions	deeper setting in the Baltic Basin
lamination	10/10 concretions	6/10 concretions	
coarse-grained laminae	0/10 concretions	4/10 concretions	storm deposits only in the shallower Lublin Basin
size of pyrite framboids	mostly <10 $\mu\text{m}$ , but variable up to 30 $\mu\text{m}$		similar redox conditions

Table 1. Comparison of sedimentological and biotic indicators of sedimentary environment between the basins

(Me) or thermal decarboxylation of kerogen (De). The concretions experienced two stages of septarian fracturing. Early septarian calcite formed still close to the sediment-water interface mainly due to BSR. Late septarian calcite precipitated at an already elevated temperature during deeper burial and became progressively enriched in Me- and De-derived DIC. These diagenetic conditions and the bitumen inclusions in the late carbonate cements suggest that biogenic methane and thermogenic hydrocarbons were liberated from the Pelplin mudstones during the early-diagenetic and burial stages, respectively.

The calcite concretions have revealed paleoecologic information about the Wenlock–Ludlow period in the Baltic and Lublin basins, which was obscured in the surrounding mudstones. The co-occurrence of early-diagenetic barite and calcite concretions with isotopic signatures indicating formation close to the sulfate-methane transition zone provides evidence of a deceleration in sedimentation during enhanced accumulation of organic matter in the basins, probably related to increased primary productivity coupled with decreased terrigenous supply. The mudstones were formed mainly by hemipelagic sedimentation in both basins, but the Lublin Basin was shallower, as indicated by the abundance of benthic fauna in concretions from this basin. Some of these conclusions may be useful for the evaluation of potential petroleum production within the interval examined, which shows that carbonate concretions are valuable sources of information not only about the diagenetic environment and pore water, but also about the major characteristics of a sedimentary basin.

## Acknowledgments

This work was supported by the Polish National Centre for Research and Development (NCRD) grant under the BLUE GAS – Polish Shale Gas program (grant no. BG1/GAZGEOLMOD/13). We thank Orlen Upstream and Polish Oil and Gas Company for granting access to core samples. We are grateful to Jim Hendry (Tullow Oil Limited, Ireland, UK) and an anonymous reviewer for their constructive comments.

## REFERENCES

- Al-Aasm, I. 2003. Origin and characterization of hydrothermal dolomite in the Western Canada Sedimentary Basin. *Journal of Geochemical Exploration*, **78-79**, 9–15.
- Azmy, K., Veizer, J., Bassett, M.G. and Copper, P. 1998. Oxygen and carbon isotopic composition of Silurian brachiopods: Implications for coeval seawater and glaciations. *Geological Society of America Bulletin*, **110**, 1499–1512.
- Baker, P.A. and Kastner, M. 1981. Constraints on the formation of sedimentary dolomite. *Science*, **213**, 214–216.
- Bennett, R.H., O'Brien, N.R. and Hulbert, M.H. 1991. Determinants of clay and shale microfabric signatures: process and mechanisms. In: Bennett, R.H., O'Brien, N.R. and Hulbert, M.H. (Eds), *Microstructure of Fine-Grained Sediments*, pp. 5–32. Springer, Berlin, Heidelberg, New York.
- Bishop, J.K.B. 1984. The barite-opal organic carbon association in oceanic particulate matter. *Nature*, **332**, 341–343.
- Blome, C.D. and Albert, N.R. 1985. Carbonate concretions: An ideal sedimentary host for microfossils. *Geology*, **13**, 212–215.
- Bojanowski, M.J. 2014. Authigenic dolomites in the Eocene–Oligocene organic carbon-rich shales from the Polish Outer Carpathians: evidence of past gas production and possible gas hydrate formation in the Silesian basin. *Marine and Petroleum Geology*, **51**, 117–135.
- Bojanowski, M.J., Barczuk, A. and Wetzel, A. 2014. Deep-burial alteration of early-diagenetic carbonate concretions formed in Palaeozoic deep-marine greywackes and mudstones (Bardo Unit, Sudetes Mountains, Poland). *Sedimentology*, **61**, 1211–1239.
- Bojanowski, M.J. and Clarkson, E.N.K. 2012. Origin of siderite concretions in microenvironments of methanogenesis developed in sulfate reduction zone: an exception or a rule? *Journal of Sedimentary Research*, **82**, 585–598.
- Bondioli, J.G., Matos, S.A., Warren, L.V., Assine, M.L., Riccomini, C. and Simões, M.G. 2015. The interplay between event and background sedimentation and the origin of fossil-rich carbonate concretions: a case study in Permian rocks of the Paraná Basin, Brazil. *Lethaia*, **48**, 522–539.
- Botor, D., Golonka, J., Zając, J., Papiernik, B. and Guzy, P. 2017. Generowanie i ekspulsja węglowodorów w utworach dolno-paleozoicznych w obszarze SW skłonu wschodnioeuropejskiej platformy prekambryjskiej w NE Polsce: implikacje dla poszukiwań złóż niekonwencjonalnych. In: Golonka, J. and Bębenek, S. (Eds), *Opracowanie map zasięgu, biostratygrafia utworów dolnego paleozoiku oraz analiza ewolucji tektonicznej przykrawędziowej strefy platformy wschodnioeuropejskiej dla oceny rozmieszczenia niekonwencjonalnych złóż węglowodorów*, pp. 423–451. Arka; Cieszyn.
- Bottrell, S.H., Parkes, J., Cragg, B.A. and Raiswell, R. 2000. Isotopic evidence for deep pyrite oxidation and stimulation of bacterial sulphate reduction. *Journal of the Geological Society*, **157**, 711–714.
- Bréhéret, J.-G. and Brumsack, H.-J. 2000. Barite concretions as evidence of pauses in sedimentation in the Marnes Bleues Formation of the Vocontian Basin (SE France). *Sedimentary Geology*, **130**, 205–228.
- Buchardt, B. and Nielsen, A.T. 1985. Carbon and oxygen isotope composition of Cambro-Silurian limestone and an-

- thraconite from Bornholm: Evidence for deep burial diagenesis. *Bulletin of the Geological Society of Denmark*, **33**, 415–435.
- Camp, W.K., Diaz, E. and Wawak, B. 2013. Electron Microscopy of Shale Hydrocarbon Reservoirs. *American Association of Petroleum Geologists Memoir*, **102**, 260 pp.
- Canfield, D.E. 2001. Biogeochemistry of sulphur isotopes. In: Valley, J.W. and Cole, D.R. (Eds), *Stable Isotope Geochemistry. Reviews in Mineralogy and Geochemistry*, pp. 607–633. Geological Society of America; Washington.
- Claypool, G.E., Holser, W.T., Kaplan, I.R., Sakai, H. and Zak, I. 1980. The age curves of sulfur and oxygen isotopes in marine sulfate and their mutual interpretation. *Chemical Geology*, **28**, 199–260.
- Cody, J.D., Hutcheon, I.E. and Krouse, H.R. 1999. Fluid flow, mixing and the origin of CO<sub>2</sub> and H<sub>2</sub>S by bacterial sulphate reduction in the Mannville Group, southern Alberta, Canada. *Marine and Petroleum Geology*, **16**, 495–510.
- Coleman, M.L. and Raiswell, R. 1993. Microbial mineralization of organic matter: mechanisms of self-organization and inferred rates of precipitation of diagenetic minerals. *Philosophical Transactions of the Royal Society A*, **344**, 69–87.
- Compton, J.S. 1988. Degree of supersaturation and precipitation of organogenic dolomite. *Geology*, **16**, 318–321.
- Cotroneo, S., Schiffbauer, J.D., McCoy, V.E., Wortmann, U.G., Darroch, S.A.F., Peng, Y. and Laflamme, M. 2016. A new model of the formation of Pennsylvanian iron carbonate concretions hosting exceptional soft-bodied fossils in Mazon Creek, Illinois. *Geobiology*, **14**, 543–555.
- Curtis, C.D. and Coleman, M.L. 1986. Controls on the precipitation of early diagenetic calcite, dolomite and siderite concretions in complex depositional sequences. In: Gautier, D.L. (Ed.), *Roles of Organic Matter during Diagenesis. SEPM Special Publication*, **38**, 23–33.
- Curtis, C.D., Coleman, M.L. and Love, L.G. 1986. Pore water evolution during sediment burial from isotopic and mineral chemistry of calcite, dolomite and siderite concretions. *Geochimica et Cosmochimica Acta*, **50**, 2321–2334.
- Davies, G.R. and Smith, L.B. 2006. Structurally controlled hydrothermal dolomite reservoir facies: an overview. *American Association of Petroleum Geologists Bulletin*, **90**, 1641–1690.
- Dean, W.E., Gardner, J.V. and Piper, D.Z. 1997. Inorganic geochemical indicators of glacial-interglacial changes in productivity and anoxia of the California continental margin. *Geochimica et Cosmochimica Acta*, **21**, 4507–4518.
- Dehairs, F., Chesselet, R. and Jedwab, J. 1980. Discrete suspended particles of barite and the barium cycle in the open ocean. *Earth and Planetary Science Letters*, **49**, 529–550.
- Delle Piane, C., Almqvist, B.S.G., MacRae, C.M., Torpy, A., Mory, A.J. and Dewhurst, D.N. 2015. Texture and diagenesis of Ordovician shale from the Canning Basin, Western Australia: Implications for elastic anisotropy and geomechanical properties. *Marine and Petroleum Geology*, **59**, 56–71.
- Dix, G.R. and Mullins, H.T. 1987. Shallow, subsurface growth and burial alteration of Middle Devonian calcite concretions. *Journal of Sedimentary Petrology*, **57**, 140–152.
- El Albani, A., Vachard, D., Kuhnt, W. and Thurow, J. 2001. The role of diagenetic carbonate concretions in the preservation of the original sedimentary record. *Sedimentology*, **48**, 875–886.
- Galimov, E.M. 1980. <sup>13</sup>C/<sup>12</sup>C in kerogen. In: Durand, B. (Ed.), *Kerogen – Insoluble Organic Matter from Sedimentary Rocks*, pp. 271–299. Editions Technip; Paris.
- Gariboldi, K., Gioncada, A., Bosio, G., Malinverno, E., Di Celma, C., Tinelli, C., Cantalamessa, G., Landini, W., Urbina, M. and Bianucci, G. 2015. The dolomite nodules enclosing fossil marine vertebrates in the East Pisco Basin, Peru: field and petrographic insights into the Lagerstätte formation. *Palaeogeography, Palaeoclimatology, Palaeoecology*, **438**, 81–95.
- Giese, U. and Köppen, S. 2001. Detrital record of Early Palaeozoic and Devonian clastic sediments at the southwestern border of the Fennoscandian Shield – provenance signals for a Caledonian geodynamic evolution. *Neues Jahrbuch für Geologie und Paläontologie-Abhandlungen*, **222**, 215–251.
- Grotek I. 2009. Petrological characteristics and thermal maturity of organic matter in Silurian sediments of the East European Craton. *Przegląd Geologiczny*, **57**, 300–301. [In Polish, summary in English]
- Heimhofer, U., Meister, P., Bernasconi, S.M., Ariztegui, D., Martill, D.M., Rios-Netto, A.M. and Schwark, L. 2017. Isotope and elemental geochemistry of black shale-hosted fossiliferous concretions from the Cretaceous Santana Formation fossil Lagerstätte (Brazil). *Sedimentology*, **64**, 150–167.
- Hendry, J.P., Pearson, M.J., Trewin, N.H. and Fallick, A.E. 2006. Jurassic septarian concretions from NW Scotland record interdependent bacterial, physical and chemical processes of marine mudrock diagenesis. *Sedimentology*, **53**, 537–565.
- Hennessy, J. and Knauth, P. 1985. Isotopic variations in dolomite concretions from the Monterey Formation, California. *Journal of Sedimentary Petrology*, **55**, 120–130.
- Hesse, R., Shah, J. and Islam, S. 2004. Physical and chemical growth conditions of Ordovician organogenic deep-water dolomite concretions: implications for the δ<sup>18</sup>O of Early Palaeozoic sea water. *Sedimentology*, **51**, 601–625.
- Hudson, J.D., Coleman, M.L., Barreiro, B.A. and Hollingworth, N.T.J. 2001. Septarian concretions from the Oxford Clay (Jurassic, England, UK): involvement of original marine and multiple external pore fluids. *Sedimentology*, **48**, 507–531.

- Irwin, H., Curtis, C. and Coleman, M. 1977. Isotopic evidence for source of diagenetic carbonates formed during burial of organic carbon-rich sediments. *Nature*, **269**, 209–213.
- Jaworowski, K. 1971. Sedimentary structures of the Upper Silurian siltstones in the Polish Lowland. *Acta Geologica Polonica*, **21**, 519–571.
- Jaworowski, K. 2000. Facies analysis of the Silurian shale-siltstone succession in Pomerania (northern Poland). *Geological Quarterly*, **44**, 297–315.
- Kiriakoulakis, K., Marshall, J.D. and Wolff, G.A. 2000. Biomarkers in a Lower Jurassic concretion from Dorset (UK). *Journal of the Geological Society*, **157**, 207–220.
- Kosakowski, P., Papiernik, B., Wróbel, M. and Machowski, G. 2015. Quantitative Description of the Selected Features of Silurian–Ordovician Shale Gas Petroleum System in Poland. In: 77<sup>th</sup> EAGE Conference and Exhibition 2015 IFE-MA Madrid, Spain, 1–4 June 2015, We P3 05.
- Lash, G.G. and Blood, D. 2004. Geochemical and textural evidence for early (shallow) diagenetic growth of stratigraphically confined carbonate concretions, Upper Devonian Rhinestreet black shale, western New York. *Chemical Geology*, **206**, 407–424.
- Lehmann, M.F., Bernasconi, S.M., Barbieri, A. and McKenzie, J.A. 2002. Preservation of organic matter and alteration of its carbon and nitrogen isotope composition during simulated and in situ early sedimentary diagenesis. *Geochimica et Cosmochimica Acta*, **66**, 3573–3584.
- Loyd, S.J., Corsetti, F.A., Eiler, J.M. and Tripathi, A.K. 2012. Determining the diagenetic conditions of concretion formation: Assessing temperatures and pore waters using clumped isotopes. *Journal of Sedimentary Research*, **82**, 1006–1016.
- Lüning, S., Craig, J., Loydell, D.K., Storch, P. and Fitches, B. 2000. Lower Silurian ‘hot shales’ in North Africa and Arabia: regional distribution and depositional model. *Earth-Science Reviews*, **49**, 121–200.
- Macquaker, J.H.S., Taylor, K.G., Keller, M. and Polya, D. 2014. Compositional controls on early diagenetic pathways in fine-grained sedimentary rocks: Implications for predicting unconventional reservoir attributes of mudstones. *American Association of Petroleum Geologists Bulletin*, **98**, 587–603.
- Majewski, W. 2000. Middle Jurassic concretions from Częstochowa (Poland) as indicators of sedimentation rates. *Acta Geologica Polonica*, **50**, 431–439.
- Malec, J., Kuleta, M. and Migaszewski, Z.M. 2016. Lithologic-petrographic characterization of Silurian rocks in the Niesztachów profile (Holy Cross Mountains). *Annales Societatis Geologorum Poloniae*, **86**, 85–110.
- Mazur, S., Mikolajczak, M., Krzywiac, P., Malinowski, M., Lewandowski, M. and Buffenmyer, V. 2016. Pomeranian Caledonides, NW Poland – A collisional suture or thin-skinned fold-and-thrust belt? *Tectonophysics*, **692**, 29–43.
- McBride, E.F. 1988. Contrasting diagenetic histories of concretions and host rock, Lion Mountain Sandstone (Cambrian), Texas. *Geological Society of America Bulletin*, **100**, 1803–1810.
- McCann, T. 1996. Silurian facies from the G-14 well, offshore Northern Germany. *Zeitschrift der Deutschen Geologischen Gesellschaft*, **147**, 209–219.
- Meister, P., Gutjahr, M., Frank, M., Bernasconi, S.M., Vasconcelos, C. and McKenzie, J.A. 2011. Dolomite formation within the methanogenic zone induced by tectonically driven fluids in the Peru accretionary prism. *Geology*, **39**, 563–566.
- Melchin, M.J., Sadler, P.M., Cramer, B.D., Cooper, R.A., Gradstein, F.M. and Hammer, O. 2012. The Silurian Period. In: Gradstein, F.M. et al. (Eds), *The Geological Time Scale 2012*, pp. 525–558. Elsevier; Amsterdam.
- Modliński, Z. 2010. Paleogeological Atlas of the sub-Permian Paleozoic of the East European Craton in Poland and neighbouring areas 1 : 2 000 000. Państwowy Instytut Geologiczny; Warszawa.
- Modliński, Z. and Podhalańska, T. 2010. Outline of the lithology and depositional features of the lower Paleozoic strata in the Polish part of the Baltic region. *Geological Quarterly*, **54**, 109–121.
- Modliński, Z., Szymański, B. and Teller, L. 2006. The Silurian lithostratigraphy of the Polish part of the Peri-Baltic depression (N Poland). *Przegląd Geologiczny*, **54**, 787–796. [In Polish, summary in English]
- Morad, S. and Eshete, M. 1990. Petrology, chemistry and diagenesis of calcite concretions in Silurian shales from central Sweden. *Sedimentary Geology*, **66**, 113–134.
- Morse, J.W. and Casey, W.H. 1988. Ostwald processes and mineral paragenesis in sediments. *American Journal of Science*, **288**, 537–560.
- Mozley, P.S. 1996. The internal structure of carbonate concretions in mudrocks: a critical evaluation of the conventional concentric model of concretion growth. *Sedimentary Geology*, **103**, 85–91.
- Mozley, P.S. and Burns, S.J. 1993. Oxygen and carbon isotopic composition of marine carbonate concretions: an overview. *Journal of Sedimentary Petrology*, **63**, 73–83.
- Page, A.A., Zalasiewicz, J.A., Williams, M. and Popov, L.E. 2007. Were transgressive black shales a negative feedback modulating glacioeustasy in the Early Palaeozoic Icehouse? In: Williams, M., Haywood, A.M., Gregory, F.J. and Schmidt, D.N. (Eds), *Deep-Time Perspectives on Climate Change: Marrying the Signal from Computer Models and Biological Proxies*, pp. 123–156. The Micropalaeontological Society, Special Publications; London.
- Passey, Q.R., Bohacs, K.M., Esch, W.L., Klimentidis, R. and Sinha, S. 2010. From oil-prone source rock to gas-producing shale reservoir – geologic and petrophysical characterization of unconventional shale-gas reservoirs, CPS/SPE International Oil and Gas Conference and Exhibition, pp. 1–29. Society of Petroleum Engineers; Beijing.

- Paytan, A., Gray, E.T., Ma, Z., Erhardt, A. and Faul, K. 2011. Application of sulphur isotopes for stratigraphic correlation. *Isotopes in Environmental and Health Studies*, **48**, 195–206.
- Paytan, A., Kastner, M. and Chavez, F.P. 1996. Glacial to interglacial fluctuations of productivity in the equatorial Pacific as indicated by marine barite. *Science*, **274**, 1355–1357.
- Paytan, A., Mearon, S., Cobb, K. and Kastner M. 2002. Origin of marine barite deposits: Sr and S isotope characterisation. *Geology*, **2002**, 747–750.
- Pearson, M.J., Hendry, J.P., Taylor, C.W. and Russell, M.A. 2005. Fatty acids in sparry calcite fracture fills and microsparite cement of septarian diagenetic concretions. *Geochimica et Cosmochimica Acta*, **69**, 1773–1786.
- Peckmann, J. and Thiel, V. 2004. Carbon cycling at ancient methane-seeps. *Chemical Geology*, **205**, 443–467.
- Peters, K.E., Walters, O.C. and Moldowan, J.M. 2005. The Biomarker Guide, 2<sup>nd</sup> edition, 471 p. Cambridge University Press; Cambridge.
- Podhalańska, T. 2009. The Late Ordovician Gondwana glaciation – a record of environmental changes in the depositional succession of the Baltic Depression (Northern Poland). *Prace Państwowego Instytutu Geologicznego*, **193**, 1–132.
- Podhalańska, T., Modliński, Z. and Szymański, B. 2010. Nowelizacja stratygrafii syluru brzeżnej części kratonu wschodnioeuropejskiego (obszar Lubelszczyzny i Podlasia). Narodowe Archiwum Geologiczne; Warszawa.
- Poprawa, P. 2006. Development of the Caledonian collision zone along the western margin of Baltica and its relation to the foreland basin. *Prace Państwowego Instytutu Geologicznego*, **186**, 189–214.
- Poprawa, P. 2010. Shale gas potential of the Lower Palaeozoic complex in the Baltic and Lublin-Podlasie basins (Poland). *Przeгляд Geologiczny*, **58**, 226–249. [In Polish, summary in English]
- Poprawa, P., Sliupa, S., Stephenson, R. and Lazauskiene, J. 1999. Late Vendian–Early Palaeozoic tectonic evolution of the Baltic Basin: regional tectonic implications from subsidence analysis. *Tectonophysics*, **314**, 219–239.
- Porębski, S.J., Prugar, W. and Zacharski, J. 2013. Silurian shales of the East European Platform in Poland – some exploration problems. *Przeгляд Geologiczny*, **61**, 468–477. [In Polish, summary in English]
- Prokoph, A., Shields, G.A. and Veizer, J. 2008. Compilation and time-series analysis of a marine carbonate  $\delta^{18}\text{O}$ ,  $\delta^{13}\text{C}$ ,  $^{87}\text{Sr}/^{86}\text{Sr}$  and  $\delta^{34}\text{S}$  database through Earth history. *Earth-Science Reviews*, **87**, 113–133.
- Raiswell, R. 1988. Evidence for surface reaction-controlled growth of carbonate concretions in shales. *Sedimentology*, **35**, 571–575.
- Raiswell, R., Bottrell, S.H., Dean, S.P., Marschall, J.D., Carr, A. and Hatfield, D. 2002. Isotopic constraints on growth conditions of multiphase calcite-pyrite-barite concretions in Carboniferous mudstones. *Sedimentology*, **49**, 237–254.
- Raiswell, R. and Fisher, J. 2000. Mudrock-hosted carbonate concretions: a review of growth mechanisms and their influence on chemical and isotopic composition. *Journal of the Geological Society*, **157**, 239–251.
- Reitner, J., Peckmann, J., Blumenberg, M., Michaelis, W., Reimer, A. and Thiel, V. 2005. Concretionary methane-seep carbonates and associated microbial communities in Black Sea sediments. *Palaeogeography, Palaeoclimatology, Palaeoecology*, **227**, 18–30.
- Riedinger, N., Kasten, S., Gröger, J., Franke, C. and Pleifer, K. 2006. Active and buried authigenic barite fronts in sediments from the Eastern Cape Basin. *Earth and Planetary Science Letters*, **241**, 876–887.
- Ritger, S., Carson, B. and Suess, E. 1987. Methane-derived authigenic carbonates formed by subduction-induced pore-water expulsion along the Oregon/Washington margin. *Geological Society of America Bulletin*, **98**, 147–156.
- Rosenbaum, J. and Sheppard, S.M. 1986. An isotopic study of siderites, dolomites and ankerites at high temperatures. *Geochimica et Cosmochimica Acta*, **50**, 1147–1150.
- Ross, D.J.K. and Bustin, R.M. 2009. The importance of shale composition and pore structure upon gas storage potential of shale gas reservoirs. *Marine and Petroleum Geology*, **26**, 916–927.
- Saigal, G.C. and Bjørlykke, K. 1987. Carbonate cements in clastic reservoir rocks from offshore Norway – relationships between isotopic composition, textural development and burial depth. In: Marshall, J.D. (Ed.), Diagenesis of Sedimentary Sequences. *Geological Society, London, Special Publications*, **36**, 313–324.
- Scotchman, I.C. 1991. The geochemistry of concretions from the Kimmeridge Clay Formation of southern and eastern England. *Sedimentology*, **38**, 79–106.
- Scotchman, I.C., Carr, A.D. and Astin, T.R. 2000. Porefluid evolution in the Kimmeridge Clay Formation of the UK Outer Moray Firth. *Journal of Geochemical Exploration*, **69–70**, 53–57.
- Sellés-Martínez, J. 1996. Concretion morphology, classification and genesis. *Earth-Science Reviews*, **41**, 177–210.
- Sirat, M., Al-Aasm, I.S., Morad, S., Aldahan, A., Al-Jallad, O., Ceriani, A., Morad, D., Mansurbeg, H. and Al-Suwaidi, A. 2016. Saddle dolomite and calcite cements as records of fluid flow during basin evolution: Paleogene carbonates, United Arab Emirates. *Marine and Petroleum Geology*, **74**, 71–91.
- Slatt, R.M. 2011. Important geological properties of unconventional resource shales. *Central European Journal of Geosciences*, **3**, 435–448.
- Strauss, H. 1997. The isotopic composition of sedimentary sulphur through time. *Palaeogeography, Palaeoclimatology, Palaeoecology*, **132**, 97–118.
- Torres, M.E., Brumsack, H.J., Bohrmann, G. and Emeis, K.C. 1996. Barite fronts in continental margin sediments: A new

- look at barium remobilisation in the zone of sulphate reduction and formation of heavy barites in diagenetic fronts. *Chemical Geology*, **127**, 125–139.
- Trela, W., Podhalańska, T., Smolarek, J. and Marynowski, L. 2016. Llandovery green/grey and black mudrock facies of the northern Holy Cross Mountains (Poland) and their relation to early Silurian sea-level changes and benthic oxygen level. *Sedimentary Geology*, **342**, 66–77.
- Wetzel, A. 1992. An apparent concretionary paradox. *Zentralblatt für Geologie und Paläontologie Teil I H*, **12**, 2823–2830.
- Whiticar, M.J., Faber, E. and Schoell, M. 1986. Biogenic methane formation in marine and freshwater environments: CO<sub>2</sub> reduction vs. acetate fermentation-Isotope evidence. *Geochimica et Cosmochimica Acta*, **50**, 693–709.
- Wiese, K. and Kvenvolden, K.A. 1993. Introduction to Microbial and Thermal Methane. In: Howell, D.G. (Ed.), The future of energy gases. *U.S. Geological Survey Professional Paper*, **1570**, 13–20.
- Więclaw, D., Kotarba, M.J., Kosakowski, P., Kowalski, A. and Grotek, I. 2010. Habitat and hydrocarbon potential of the Lower Paleozoic source rocks in the Polish part of the Baltic region. *Geological Quarterly*, **54**, 159–182.
- Wignall, P. B. and Newton, R. 1998. Pyrite framboid diameter as a measure of oxygen deficiency in ancient mudrocks. *American Journal of Science*, **298**, 537–552.
- Wilkin, R.T., Barnes, H.L. and Brantley, S.L. 1996. The size distribution of framboidal pyrite in modern sediments: An indicator of redox conditions. *Geochimica et Cosmochimica Acta*, **60**, 3897–3912.

*Manuscript submitted: 5<sup>th</sup> April 2018*

*Revised version accepted: 9<sup>th</sup> November 2018*

**Suppl. Tab. 1.** Results of XRD analyses depicting the mineral composition of mudstones and concretions with contents of minerals given in wt%

Basin	Sample	Material	Calcite	Dolomite	Quartz	Albite	Ortoclase	2:1 layer phyll.	Kaolinite	Chlorite	Pyrite	Gypsum	Barite	Dolomite/ calcite	Quartz/ 2:1 layer phyll.
	Be1m	mudstone	7.3	16.6	23.7	12.7		21.3		15.7	2.6			2.3	1.1
	Be1e	concretion matrix	78.1	3.7	13.8	1.9		2.3			0.2			0.0	
	Be1g	concretion matrix	85.1	3.3	7.1	1.5		2.8			0.2			0.0	
	Do1m	mudstone	0.7	0.3	28.6	15.1		20.3		21.1	13.9			0.4	1.4
	Do1b	concretion matrix	72.8		16.3	4.8		3.7			2.5			0.0	
	Do1e	concretion matrix	89.2		6.6	2.3		0.4		1.2	0.3			0.0	
	Do2m	mudstone	6.7	0.3	27.3	13.8	5.2	19.4		19.7	7.6			0.0	1.4
L	Do2d	concretion matrix	84.6		9.6	3.9		0.3		1.3	0.4			0.0	
	Do2e	concretion matrix	75.5		11.6	5.7		3.5		2.0	1.7			0.0	
U	Do2f	concretion matrix	81.3		9.9	3.9		0.5		2.5	1.9			0.0	
	Do2g	concretion matrix, edge	67.7		13.7	6.5		6.9		3.9	1.3			0.0	
	Do3m	mudstone	43.1	1.5	11.3	8.4	6.6	13.6		14.0	1.5			0.0	0.8
B	Do3e	concretion matrix	80.0	3.5	9.8	3.7		2.4			0.7			0.0	
	Do4m	mudstone	5.0	13.1	24.1	11.6	6.1	14.2	7.6	14.8	3.6			2.6	1.7
L	Do4d	concretion matrix with barite domain	82.6	2.2	5.1	0.9		0.7			1.4		7.1	0.0	
	Do4g	concretion matrix	78.8	2.5	11.3	4.1		3.0			0.3			0.0	
I	Sy1m	mudstone	10.4	0.7	28.1	10.7	6.8	19.9		19.1	4.4			0.1	1.4
	Sy1b	concretion matrix	91.3	0.1	7.8	0.8								0.0	
	Sy1e	concretion matrix	88.8		6.6	0.9		2.0		1.7				0.0	
N	Sy2m	mudstone	0.7	1.0	27.6	10.0	6.1	32.1		12.2	8.2	2.1		1.5	0.9
	Sy2e	concretion matrix	75.8		11.3	2.7		4.1		4.5	1.7			0.0	
	Sy3m	mudstone	5.8	0.8	29.5	13.0	7.9	18.3		20.8	4.0			0.1	1.6
	Sy3c	concretion matrix	86.6	1.2	8.2	1.3		1.0		1.4	0.4			0.0	
	Sy4m	mudstone	3.4	10.0	26.9	9.1	8.4	25.8		13.9	2.5			2.9	1.0
	Sy4b	concretion matrix	77.8	3.3	9.7	1.0		4.0		3.9	0.3			0.0	
	Sy5m	mudstone	6.8	9.4	22.9	9.4	8.5	22.2		17.6	3.3			1.4	1.0
	Sy5e	concretion matrix	85.2	1.4	9.9	0.4		2.5			0.6			0.0	
<i>average</i>															<i>1.2</i>
	Bo1m	mudstone	1.5	1.2	38.7	12.8		23.2		19.5	3.1			0.8	1.7
	Bo1g	concretion matrix	81.0	2.0	10.4	1.8		4.5			0.5			0.0	
	Bo2m	mudstone	8.6	5.1	39.1	9.4	4.8	13.1	2.8	14.5	2.7			0.6	3.0
B	Bo2b	concretion matrix	77.5	3.8	12.4	1.3		4.4			0.6			0.0	
	Bo3m	mudstone	5.7	3.7	34.7	11.0	5.8	17.4		18.3	3.5			0.6	2.0
	Bo3b	concretion matrix	74.2	3.1	11.8	1.8		5.0		3.8	0.4			0.0	
A	Bo4b	concretion matrix	77.8	2.2	10.9	1.6		6.6			0.9			0.0	
	Bo5m	mudstone	8.3	4.4	33.6	10.6		19.1		19.6	4.4			0.5	1.8
L	Bo5f	concretion matrix	78.8	0.7	12.0	0.9		6.0			1.5			0.0	
	Ko1m	mudstone	9.1	8.4	35.0	8.2	4.8	20.0		12.0	2.5			0.9	1.7
	Ko1e	concretion matrix	73.2	1.5	11.7	2.4		6.4		4.1	0.7			0.0	
T	Op1m	mudstone	4.8	6.9	30.4	10.2	5.1	25.3		15.0	2.4			1.4	1.2
	Op1c	concretion matrix	72.9	1.5	12.8	2.8		6.2		3.8				0.0	
I	Op1d	concretion matrix	80.8	0.9	9.3	2.6		3.3		2.5	0.5			0.0	
	Wy1m	mudstone	0.6	1.7	29.3	12.4	6.1	24.3		20.3	5.3			2.9	1.2
C	Wy1f	concretion matrix	83.0	1.2	7.7	2.0		3.0		2.1	1.0			0.0	
	Wy2m	mudstone	2.7	7.7	31.0	8.9	6.7	26.8		12.8	3.4			2.9	1.2
	Wy2b	concretion matrix	80.9	2.4	9.2	1.5		4.3		1.5	0.3			0.0	
	Wy3m	mudstone	9.8	5.2	37.4	10.2		18.4		14.7	4.4			0.5	2.0
	Wy3i	concretion matrix	80.5	2.5	10.8	1.2		1.3		2.7	1.0			0.0	
<i>average</i>															<i>1.8</i>



**Suppl. Tab. 3.** Results of SEM-EDS analyses depicting the elemental composition of carbonate components

Rock type	Material	n	CaCO <sub>3</sub> [mol%]				MgCO <sub>3</sub> [mol%]				MnCO <sub>3</sub> [mol%]				FeCO <sub>3</sub> [mol%]			
			mean	sd	min	max												
Mudstones	silt-sized calcite (intraclasts?) in mudstones	6	89.7	1.3	87.9	91.1	6.6	1.2	5.4	8.2	b.d.	-	b.d.	b.d.	3.7	0.2	3.3	4.0
	dolomite	8	62.2	4.2	55.4	67.2	35.2	4.0	30.4	40.5	0.0	0.1	b.d.	0.2	2.5	0.8	1.6	4.1
	microspar cement in mudstones	11	92.7	0.9	91.4	93.7	4.9	0.7	4.0	5.9	0.2	0.1	b.d.	0.3	2.3	0.3	1.9	2.8
	cement in microfossils in mudstones	3	92.4	0.2	92.3	92.7	5.1	0.2	4.9	5.3	0.3	0.0	0.3	0.4	2.1	0.1	2.0	2.1
C o n c r e t i o n s	cement in microfossils in concretions	6	96.8	0.7	96.0	97.7	2.2	0.6	1.4	3.0	0.5	0.3	b.d.	0.7	0.6	0.2	0.3	0.9
	shells of benthic macrofossils	26	96.5	0.8	94.6	98.2	2.4	0.7	1.1	3.7	0.3	0.1	b.d.	0.4	0.8	0.3	0.3	1.3
	shells of nectic macrofossils	11	96.9	0.9	95.7	98.1	2.2	0.6	1.2	2.9	0.2	0.1	b.d.	0.4	0.7	0.3	0.4	1.1
	calcified spicules	10	96.0	0.9	94.9	97.6	2.8	0.9	1.2	3.9	0.3	0.2	b.d.	0.5	0.9	0.2	0.7	1.2
	tubular shells	2	95.0	0.1	94.9	95.1	3.6	0.1	3.6	3.7	0.4	0.0	0.4	0.4	1.0	0.0	1.0	1.0
	echinoderm fragments	2	94.2	1.4	93.2	95.2	3.5	1.0	2.9	4.2	0.5	0.1	0.4	0.6	1.8	0.4	1.6	2.1
	intrashell calcite cement	68	96.5	1.3	93.4	98.8	2.7	1.3	0.9	5.6	0.3	0.2	b.d.	0.6	0.5	0.4	b.d.	1.8
	saddle ankerite	2	59.1	2.4	57.4	60.8	25.0	0.7	24.5	25.5	2.1	0.2	2.0	2.2	13.8	1.5	12.8	14.9
	intergranular sparite	5	97.4	0.7	96.4	98.1	1.9	0.2	1.7	2.2	0.2	0.3	b.d.	0.7	0.5	0.4	b.d.	1.1
	concretionary microspar	69	94.9	1.3	92.4	97.8	3.9	1.2	1.2	5.9	0.2	0.2	b.d.	0.6	0.9	0.3	0.4	1.9
	septarian calcite - 1st generation	16	96.6	0.9	95.4	98.0	2.7	1.3	0.9	4.2	0.6	0.5	b.d.	1.6	0.1	0.1	b.d.	0.3
	septarian calcite - 2nd generation	6	96.6	0.8	96.0	98.1	2.4	0.6	1.2	2.7	0.4	0.2	0.2	0.6	0.6	0.2	0.5	0.9
	calcite replacing barite	27	95.4	0.8	94.2	97.3	3.0	1.1	1.3	5.0	0.5	0.4	b.d.	1.5	1.0	0.4	0.5	2.3

*b.d.* - below detection

Suppl. Tab. 4. Results of isotopic measurements. O isotope values of mudstones were corrected for dolomite fractionation effect proportionally to dolomite/calcite ratio.

L U B L I N B A S I N

B A L T I C B A S I N

Sample	Material	$\delta^{13}\text{C}_{\text{carb}}$ [‰]	$\delta^{18}\text{O}_{\text{carb}}$ [‰]	$\delta^{13}\text{C}_{\text{org}}$ [‰]	$\delta^{34}\text{S}_{\text{sulf}}$ [‰]	$\delta^{18}\text{O}_{\text{sulf}}$ [‰]	Age
Be1m	mudstone	-0.4	-6.5	-29.0			Homerian
Be1a	concretion matrix	-6.5	-3.6				
Be1b	concretion matrix	-6.9	-3.9				
Be1c	concretion matrix	-7.5	-4.0				
Be1d	concretion matrix	-7.8	-4.1				
Be1e	concretion matrix	-7.0	-5.7				
Be1f	concretion matrix	-7.8	-4.2				
Be1g	concretion matrix	-7.3	-3.9				
Be1h	concretion matrix	-7.7	-4.6				
Be1i	concretion matrix	-12.2	-5.3				
Be1s1	1 <sup>st</sup> gen. of septarian calcite	-9.6	-6.0				
Be1s2	2 <sup>nd</sup> gen. of septarian calcite	-8.5	-12.4				
		<i>r</i>	0.51				
Do1m	mudstone	0.6	-10.4	-30.3			Ludfordian
Do1a	concretion matrix	-2.6	-10.9				
Do1b	concretion matrix	-4.7	-10.5				
Do1c	matrix with coarse-grained material	-5.6	-9.2				
Do1d	concretion matrix	-5.9	-10.7				
Do1e	concretion matrix	-4.9	-10.6				
Do1f	concretion matrix	-5.4	-10.5				
Do1g	concretion matrix	-5.8	-10.4				
Do1h	concretion matrix	-3.8	-10.8				
Do1i	concretion matrix	-1.2	-11.1				
Do1s	2 <sup>nd</sup> gen. of septarian calcite	-5.3	-10.6				
		<i>r</i>	-0.56				
Do2m	mudstone	-2.2	-11.5	-30.2			Ludfordian
Do2a	concretion matrix	-1.3	-11.4				
Do2b	concretion matrix	-2.6	-10.5				
Do2c	concretion matrix	-5.1	-10.4				
Do2d	concretion matrix	-5.3	-10.7				
Do2e	concretion matrix	-5.0	-10.6				
Do2f	concretion matrix	-2.1	-11.1				
Do2g	concretion matrix	-1.3	-11.4				
Do2s	1 <sup>st</sup> gen. of septarian calcite	-2.2	-5.6				
		<i>r</i>	-0.84				
Do3m	mudstone	-2.1	-10.5	-30.9			Sheinwoodian
Do3a	concretion matrix	-14.3	-10.3				
Do3b	concretion matrix	-12.8	-10.1				
Do3c	concretion matrix	-12.6	-10.1				
Do3d	concretion matrix	-12.8	-10.2				
Do3e	concretion matrix	-13.0	-10.1				
Do3s	1 <sup>st</sup> gen. of septarian calcite	-6.9	-6.2				
		<i>r</i>	0.65				
Do4m	mudstone	-0.7	-7.7	-30.6			Sheinwoodian
Do4a	concretion matrix	-10.9	-9.9				
Do4b	concretion matrix	-11.1	-10.1				
Do4c	concretion matrix	-11.2	-10.2				
Do4d	matrix with barite domain	-11.7	-10.2				
Do4e	concretion matrix	-11.8	-10.3				
Do4f	concretion matrix	-11.7	-10.2				
Do4g	concretion matrix	-11.8	-10.0				
Do4h	concretion matrix	-11.6	-10.0				
Do4s	1 <sup>st</sup> gen. of septarian calcite	-9.2	-4.5				
		<i>r</i>	0.48				
Sy1m	mudstone	0.5	-8.5	-30.1			Ludfordian
Sy1a	concretion matrix	-3.3	-5.9				
Sy1b	concretion matrix	-1.4	-5.8				
Sy1c	matrix with coarse-grained material	-1.2	-4.4				
Sy1d	concretion matrix	-3.7	-6.3				
Sy1e	concretion matrix	-3.5	-6.5				
Sy1f	concretion matrix	-1.9	-7.3				
		<i>r</i>	0.45				
Sy2m	mudstone	-1.1	-9.6	-30.1			Ludfordian
Sy2a	concretion matrix	-0.5	-7.6				
Sy2b	concretion matrix	-1.2	-7.7				
Sy2c	matrix with coarse-grained material	-2.6	-5.5				
Sy2d	concretion matrix	-2.4	-7.4				
Sy2e	concretion matrix	-0.6	-7.3				
Sy2f	concretion matrix	-0.9	-7.8				
Sy2g	concretion matrix	-0.9	-8.5				
		<i>r</i>	-0.65				
Sy3m	mudstone	-1.1	-9.3	-30.1			Ludfordian
Sy3a	concretion matrix	-0.5	-7.0				
Sy3b	concretion matrix	-0.5	-7.0				
Sy3c	concretion matrix	-0.1	-7.1				
Sy3d	concretion matrix	-0.6	-7.2				
Sy3e	concretion matrix	-0.5	-7.0				
		<i>r</i>	-0.16				
Sy4m	mudstone	-0.9	-6.2	-31.5			Sheinwoodian
Sy4a	barite crystals				36.7		
Sy4b	concretion matrix	-10.2	-6.9				
Sy4c	concretion matrix	-9.2	-7.1				
Sy4d	concretion matrix	-8.9	-7.1				
Sy4e	concretion matrix	-9.1	-7.1				
Sy4f	concretion matrix	-10.4	-6.6				
Sy4g	barite crystals				63.7		
Sy4h	concretion matrix	-12.7	-6.6				
Sy4i	concretion matrix	-13.7	-7.3				
		<i>r</i>	-0.07				
Sy5m	mudstone	-0.4	-7.3	-30.8			Sheinwoodian
Sy5a	concretion matrix	-9.4	-6.6				
Sy5b	concretion matrix	-11.7	-6.7				
Sy5c	concretion matrix	-11.7	-6.9				
Sy5d	concretion matrix	-11.4	-7.0				
Sy5e	concretion matrix	-11.1	-6.9				
Sy5f	concretion matrix	-10.9	-6.5				
Sy5g	concretion matrix	-9.9	-6.9				
Sy5h	concretion matrix	-9.4	-6.6				
Sy5i	concretion matrix	-9.5	-6.8				
Sy5j	barite domain				43.8		
Sy5s1	1 <sup>st</sup> gen. of septarian calcite	-10.0	-3.5				
Sy5s2	2 <sup>nd</sup> gen. of septarian calcite	-2.7	-5.6				
Sy5s3	septarian barite				42.7	16.6	
		<i>r</i>	0.33				
	average	-6.7	-8.0				

*r* - correlation coefficient between  $\delta^{13}\text{C}$  and  $\delta^{18}\text{O}$  calculated for matrix samples of each concretion

Sample	Material	$\delta^{13}\text{C}_{\text{carb}}$ [‰]	$\delta^{18}\text{O}_{\text{carb}}$ [‰]	$\delta^{13}\text{C}_{\text{org}}$ [‰]	$\delta^{34}\text{S}_{\text{sulf}}$ [‰]	$\delta^{18}\text{O}_{\text{sulf}}$ [‰]	Age
Bo1m	mudstone	-1.1	-8.2	-30.2			Gorstian
Bo1a	concretion matrix	-19.4	-5.7				
Bo1b	concretion matrix	-18.8	-5.5				
Bo1c	concretion matrix	-17.6	-5.4				
Bo1d	concretion matrix	-17.9	-5.6				
Bo1e	concretion matrix	-18.9	-5.7				
Bo1f	concretion matrix	-16.5	-5.4				
Bo1g	concretion matrix	-14.2	-5.2				
Bo1h	concretion matrix	-12.6	-5.0				
Bo1i	concretion matrix	-11.4	-4.7				
		<i>r</i>	0.97				
Bo2m	mudstone	-2.7	-8.2	-30.4			Homerian
Bo2a	concretion matrix	-20.2	-6.6				
Bo2b	concretion matrix	-20.5	-6.5				
Bo2c	concretion matrix	-20.7	-6.6				
Bo2d	concretion matrix	-20.6	-6.7				
Bo2e	concretion matrix	-20.7	-6.8				
Bo2f	concretion matrix	-20.9	-7.0				
Bo2g	concretion matrix	-20.2	-7.2				
		<i>r</i>	-0.04				
Bo3m	mudstone	-1.2	-7.5	-30.1			Sheinwoodian
Bo3a	concretion matrix	-20.1	-6.1				
Bo3b	concretion matrix	-19.5	-6.0				
Bo3c	concretion matrix	-18.6	-5.7				
Bo3d	concretion matrix	-18.2	-5.7				
Bo3e	concretion matrix	-17.4	-5.6				
Bo3f	concretion matrix	-17.3	-5.6				
Bo3g	concretion matrix	-17.9	-5.7				
Bo3h	concretion matrix	-18.2	-5.8				
Bo3i	concretion matrix	-18.2	-5.8				
		<i>r</i>	0.90				
Bo4a	concretion matrix	-20.9	-5.8	-27.3			Sheinwoodian
Bo4b	concretion matrix	-20.8	-5.8				
Bo4c	concretion matrix	-20.9	-5.8				
Bo4d	concretion matrix	-20.4	-5.6				
Bo4e	concretion matrix	-20.6	-5.4				
Bo4f	concretion matrix	-20.4	-5.5				
Bo4g	concretion matrix	-20.5	-5.5				
Bo4h	concretion matrix	-20.7	-5.6				
Bo4i	concretion matrix	-20.9	-5.7				
		<i>r</i>	0.76				
Bo5m	mudstone	-0.5	-8.0	-28.4			Sheinwoodian
Bo5a	concretion matrix	-3.6	-5.1				
Bo5b	concretion matrix	-6.5	-5.0				
Bo5c	concretion matrix	-7.0	-4.9				
Bo5d	concretion matrix	-8.2	-4.8				
Bo5e	concretion matrix	-8.5	-4.7				
Bo5f	concretion matrix	-8.5	-4.8				
Bo5g	concretion matrix	-7.2	-5.0				
Bo5h	concretion matrix	-6.5	-5.0				
Bo5i	concretion matrix	-4.0	-5.5				
		<i>r</i>	-0.88				
Ko1m	mudstone	-1.2	-7.4	-31.6			Homerian
Ko1a	concretion matrix	-20.3	-7.0				
Ko1b	concretion matrix	-21.4	-6.8				
Ko1c	concretion matrix	-22.3	-6.9				
Ko1d	concretion matrix	-23.5	-6.8				
Ko1e	concretion matrix	-23.9	-6.7				
Ko1f	concretion matrix	-22.5	-6.7				
Ko1g	concretion matrix	-21.2	-6.8				
Ko1h	concretion matrix	-20.0	-7.0				
Ko1i	concretion matrix	-18.5	-7.5				
		<i>r</i>	-0.86				
Op1m	mudstone	-0.6	-6.5	-29.3			Homerian
Op1a	concretion matrix	-18.7	-5.6				
Op1b	concretion matrix	-19.0	-5.4				
Op1d	concretion matrix	-19.2	-5.2				
Op1c	concretion matrix	-17.2	-4.7				
Op1e	concretion matrix	-18.0	-5.1				
Op1f	concretion matrix	-18.9	-5.3				
Op1g	concretion matrix	-18.5	-5.4				
Op1h	concretion matrix	-12.4	-5.5				
Op1s1	1 <sup>st</sup> gen. of septarian calcite	-13.1	-5.0				
Op1s2	2 <sup>nd</sup> gen. of septarian calcite	-3.5	-12.7				
		<i>r</i>	-0.18				
Wy1m	mudstone	-0.8	-7.3	-29.4			Homerian
Wy1a	concretion matrix	-12.3	-5.9				
Wy1b	concretion matrix	-9.3	-5.9				
Wy1c	concretion matrix	-9.7	-6.1				
Wy1d	concretion matrix	-8.9	-6.0				
Wy1e	concretion matrix	-9.6	-6.1				
Wy1f	concretion matrix	-8.9	-5.9				
Wy1g	concretion matrix	-11.8	-5.9				
Wy1s1	1 <sup>st</sup> gen. of septarian calcite	-7.0	-10.2				
Wy1s2	2 <sup>nd</sup> gen. of septarian calcite	4.1	-11.5				
		<i>r</i>	-0.42				
Wy2m	mudstone	-0.2	-5.8	-29.0			Sheinwoodian
Wy2a	concretion matrix	-16.3	-6.0				
Wy2b	concretion matrix	-15.2	-6.3				
Wy2c	concretion matrix	-15.8	-6.2				
Wy2d	concretion matrix	-15.4	-5.8				
Wy2e	concretion matrix	-15.3	-5.9				
Wy2f	concretion matrix	-15.8	-5.8				
Wy2g	concretion matrix	-15.3	-6.8				
Wy2s	septarian barite				13.7	13.5	
		<i>r</i>	-0.32				
Wy3m	mudstone	-0.7	-7.8	-27.6			Sheinwoodian
Wy3a	concretion matrix	-8.5	-6.4				
Wy3b	concretion matrix	-9.2	-6.6				
Wy3c	concretion matrix	-10.1	-6.2				
Wy3d	concretion matrix	-11.4	-6.0				
Wy3e	concretion matrix	-12.6	-6.0				
Wy3f	concretion matrix	-13.1	-6.1				
Wy3g	concretion matrix	-12.3	-6.0				
Wy3h	concretion matrix	-11.8	-6.1				
Wy3i	concretion matrix	-11.0	-6.1				
Wy3j	concretion matrix	-10.7	-6.4				
Wy3k	concretion matrix	-10.4	-6.4				
		<i>r</i>	-0.84				
	average	-15.7	-5.9	</			